Dry granular flows down an inclined channel: Experimental investigations on the frictional-collisional regime

Christophe Ancey
Cemagref, Division ETNA, Domaine Universitaire, BP 76, 38402 Saint-Martin-d'Hères Cedex, France
(Received 3 January 2001; revised manuscript received 18 June 2001; published 18 December 2001)

This paper presents experimental results on dry granular flows down an inclined rough channel. Different flow regimes were identified depending on the Froude number. For Froude numbers exceeding a critical value (function of the channel slope), flow was characterized by a fairly linear velocity profile and a discharge equation in the form $q \propto h^n$ with q the flow rate per unit width, h the flow depth, and n an exponent in the range 2–3 (regime A). When the Froude number was lower than the critical value, the flow was characterized by a convex velocity profile and a discharge equation of the form $q \propto h^n$, with n ranging from 0.97 to 1.16, producing the striking result that the mean velocity was constant for a given inclination of the channel (regime B). Experimental data were used to test three theoretical models developed to describe dry granular flows in a frictional-collisional regime. Savage's model provides results that capture experimental trends well and yield the correct magnitude for velocity and discharge for regime A, but it reproduces the dependence of the discharge on the channel slope for only a narrow range of slopes [S. B. Savage, in *U.S./Japan Seminar on New Models and Constitutive Relations in the Mechanics of Granular Materials, Ithaca, 1982*, edited by J. T. Jenkins and M. Satake (Elsevier Science Publishers, Amsterdam, 1982), p. 261]. In contrast, Mills *et al.*'s model is less refined and requires fitting an input parameter to give the correct magnitude of velocity but it successfully accounts for the variation in the discharge with slope for regime A for a wide range of slopes [Mills, Loggia, and Tixier, Europhys. Lett. **45**, 733 (1999); Eur. Phys. J. E **1**, 5 (2000)]. Ancey and Evesque's model is also crude in determining the density profile but manages to provide velocity profiles and discharge equations in good agreement with experimental data for regime B [C. Ancey and P. Evesque, Phys. Rev. E **62**, 8349 (2000)].

DOI: 10.1103/PhysRevE.65.011304 PACS number(s): 45.70.−n, 45.50.−j, 83.10.Gr

I. INTRODUCTION

This paper presents an experimental investigation into dry granular flows down an inclined channel, with specific attention directed to the frictional-collisional regime. Here the term ''dry granular flows'' refers to flows of a granular suspension made up of solid particles in air. The solid concentration ϕ defined as the ratio of solid volume to total volume is high, basically higher than 50% on average. The typical particle size is assumed to be sufficiently large for the electrostatic effects and air fluidization to be negligible. Particles interact with each other in various ways: through sustained contacts, which transmit forces throughout the bulk, or by instantaneous contacts, which produce an exchange of momentum between particles. The former type of contact is usually called ''frictional contact'' while the second is referred to as ''collisional contact.'' Here the frictional-collisional regime corresponds to a flow regime where bulk stress results from the combination of collisional and frictional contacts. Dimensional analysis can be helpful in delineating the flow regimes using dimensionless groups (see [1,2]). This can be done, for example, using the Coulomb number, defined as the ratio of collision magnitude to the typical stress Σ acting on particles: $N_{Co}=\rho_p a^2 \Gamma^2/\Sigma$, where Γ is the mean shear rate, ρ_p is the particle density, a is the particle radius. The frictional-collisional regime is expected to occur when $N_{Co}=O(1)$.

Such a regime is an intermediate stage between the frictional and collisional regimes. For a purely frictional regime (also called ''quasistatic'' or ''rate-independent plastic'') $N_{Co} \ll 1$, bulk behavior is generally described within the soil-mechanics framework by using empirical models or homogenization techniques. In a simple shear flow, it is found that for sufficiently large deformations, the shear stress τ is independent of the shear rate and is linearly linked to the normal stress σ [3]. The resulting relationship is known as the Coulomb law: $\tau=|\sigma|\tan\varphi$, where φ, called the *internal friction angle*, is a parameter intrinsic to the material. Frictional behavior originates at the particle scale from sustained frictional contacts between closely packed particles [4,5]. For a collisional regime $N_{Co} \gg 1$, (also called ''grain-inertia regime'' in reference to the pioneering work of Bagnold [6]), bulk behavior is usually described using kinetic theories, which are based on an analogy with gases [7]. In a simple shear flow, the shear stress τ is linked to the shear rate $\dot{\gamma}$ through a viscosity term η, which depends on the particle velocity fluctuation strength: $\tau=\eta(T)\dot{\gamma}$, where $T=\langle \mathbf{u}' \cdot \mathbf{u}' \rangle$, called the *granular temperature*, is the square root mean of the velocity fluctuations $\mathbf{u}'$. Furthermore, it is generally found that for a simple shear flow the viscosity varies as the shear rate and thus the shear stress is a quadratic function of the shear rate.

Relatively little is known on the frictional-collisional regime from both theoretical and experimental points of view. Conceptually, the mere idea that collisional and frictional contacts coexist at high solid fractions may be seen as paradoxical. Indeed, for collisional contacts to be an efficient mechanism in bulk stress generation, the motion of particles through the bulk must not be too impeded and contacts must be of short duration. Conversely, for frictional contacts to

 ©2001 The American Physical Society

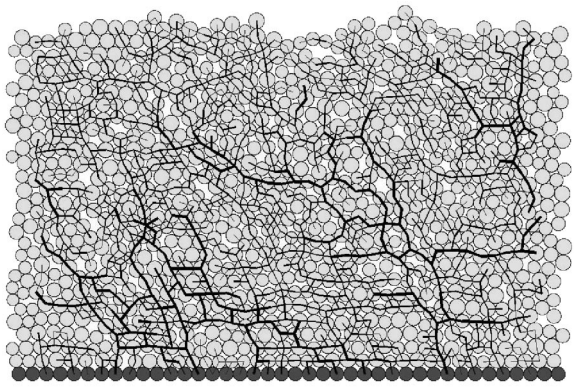

FIG. 1. Normal force diagram in a dry granular flow (courtesy of F. Chevoir and M. Prochnow, LMSGC, Champs sur Marne, France). The line thickness is proportional to the force strength. The material is made up of polydisperse disks (uniform distribution in size ranging from $0.85R$ to $1.15R$). The channel slope is $18°$. The Coulombic friction coefficient is $f=0.4$. The tangential and normal restitution coefficients are zero.

influence bulk stress, particles must be closely packed with contacts of long duration. Recent experiments and numerical simulations have contributed to clarifying this paradox. They have shown that at any time in a simple shear flow (i) networks of particles in close contact cover the flowing layer, (ii) they transmit strong forces, and (iii) they surround particle clusters, where the stress level is much lower. Particles belonging to a force network experience sustained frictional forces (''strong population''), while particles in clusters (''weak population'') are mainly subjected to collisions. Figure 1 depicts a typical distribution of contact forces within a granular flow down an inclined channel, obtained by Prochnow and co-workers [8] using a contact dynamics numerical scheme. Likewise, Capart and his co-workers [9] measured the particle velocity and granular temperature for different kinds of water-saturated mixtures of cylinder-shaped polyvinyl chloride (PVC) granules flowing down an inclined channel. They observed regions where the granular temperature was fairly high and mean velocities were not well correlated, and other regions where the correlation in the mean particle velocity was significantly enhanced and granular temperature was decreased.

From an experimental point of view, one is faced with various difficulties when investigating the rheological properties of a frictional-collisional regime. So far annular shear cells (a variant of the parallel-plate rheometer) and inclined channels have been the most common geometries used to infer the constitutive characteristics of granular suspensions. An annular shear cell benefits from a simple viscometric treatment since the shear-rate and stress distributions are normally known in advance. However, in practice, various disturbing effects (shear-rate localization, stick-slip behavior, etc.) limit the advantage of this geometry for granular flows. The origins of these disturbing effects have been partially explained. For instance, by simulating a shearing box whose upper boundary sheared arrays of disks at constant volume, Aharonov and Sparks [10] observed intermittent networks due to grain jamming, resulting in a stick-slip motion. In contrast, due to the free surface that allows dilatancy, granular flows down an inclined channel are not subjected to such disturbing effects, but contrary to the annular shear cell, the shear rate cannot be imposed.

To date, few experiments have been carried out with the objective of determining the rheological properties of granular flows in a frictional-collisional regime. It is well known that the type of bottom roughness significantly affects the nature and structure of flow. For a smooth bottom and shallow flows, the material flows as a diffuse, low-density layer of strongly agitated particles while, for increasing flow depth, a ''locked'' flow occurs with a high slip velocity at the base and a vanishing shear rate inside the flowing material [11]. For a rough bottom, a sheared flow occurs with a low slip velocity at the base. Most experimental research has focused on channels with a smooth base, most of the time in order to investigate the collisional regime [11–21]. Only a few authors used inclined channels with a rough bottom. Using a 1.2-m-long channel, Suzuki and Tanaka [22] carried out tests on calcite, sand, and glass beads. They found that a viscoplastic Bingham model could be used as a constitutive equation. In fact, owing to the narrow range of flow rates, a linear relationship between discharge and flow depth fit their data better and thus their conclusion was probably erroneous. Using a 1.2-m-long channel and polystyrene beads 1.2 mm in diameter, Savage measured the free surface profile [23]. The velocity profile at the sidewall and the free surface was measured using two fiber optic probes and signal correlation techniques. The velocity profiles measured at three slopes ($32.6°$, $35.3°$, and $39.3°$) were convex, with an inflection point near the free surface. He gave some data concerning the discharge equation. From these data, we can deduce that it was nearly linear. Velocity profiles were also measured by Ishida and co-workers [24–26]. The channel was 0.954 m long and its base was roughened using sand paper. They used three types of particle: sand grain (0.19 mm), glass bead (0.35–0.5 mm), and alumina powder (0.23 mm). The base was aerated by injecting a flow rate of air through a porous bed. The profiles were slightly convex for lower channel slopes ($24°$) and tended toward a linear profile for increasing slopes ($30°$). No slip was observed at the bottom. Vallance [27] used a rough channel 1.2 m in length and 7.5 cm in width. Using both a trapping system and image processing, he observed that the velocity profile was slightly convex at the sidewall but linear inside the flow. For low inclinations and flow depths h, the discharge q varied as $h^{5/2}$ while for thick flows and slope in excess of a critical value close to the internal friction angle, the discharge varied as $h^{3/2}$ [27]. Using glass beads and a narrow channel (2.5 cm wide), Ancey and co-workers [28] found that for sufficiently large discharges, the mass flow rate was linearly dependent on the flow depth for slopes ranging from $25°$ to $37°$. Pouliquen [29] used a very wide (0.7 m) plane 2 m in length. The material was glass beads with the diameter ranging from 0.5 mm to 1.3 mm. After releasing the material contained in a box, he measured the velocity of the front using an image-processing system. Within the range of slope $20°–28°$, he found that the mean velocity at the leading edge varied as $\ln|\theta-\varphi|h^{3/2}$. Using a 4-m-long channel and 3-mm glass

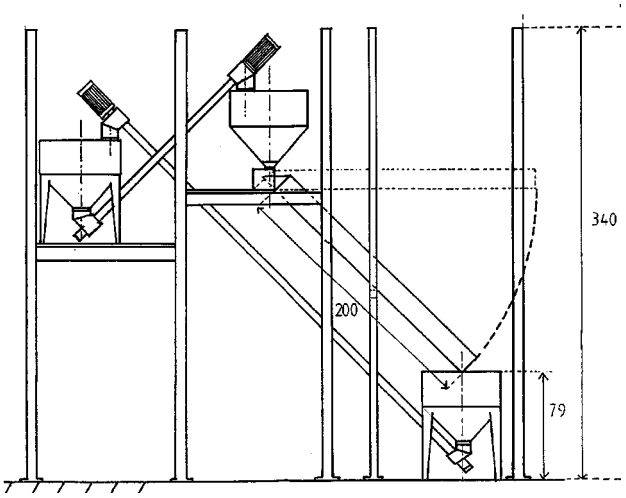

FIG. 2. Schematic view of the channel used.

beads, Hanes and Walton observed the collisional regime only for a narrow range of channel slopes (around 23 °) [30].

In addition, a few experiments have been performed using a two-dimensional channel. Drake [31,32] used a 3.7-m-long and 3.25-cm-wide channel and acetate beads (6 mm in diameter). Measuring the velocity and density profiles, he showed that flow could be divided into three layers: a slipping layer near the bottom, a chaotic zone, and a saltation layer near the free surface. Azanza and co-workers ran similar experiments and compared their data with predictions from a kinetic theory [33]; partial agreement was found when flow was dilute (i.e., near the free surface). On the whole, all these experiments endeavored to measure a few quantities (velocity profile, density profile, etc.) in a narrow range of flow conditions without providing a comprehensive picture of the flow pattern (flow regimes, discharge equation, etc.). This perhaps explains why they are not always consistent when compared with each other. For instance, in the case of dry granular flows down inclined channels, authors found that, for a steady uniform flow, the discharge equation was: $q \propto h^{2.5}$ (with h the flow depth and q the flow rate) [29] whereas others found a relation in the form of $q \propto h$ [28].

The present paper reports an investigation of the flow properties of dry granular flows down an inclined channel. To supplement the detailed experiments performed by Johnson, Nott, and Jackson [11] on dry granular flows down smooth chutes, here we focus our attention on flows down a rough bottom. First we will describe the materials used and the experimental procedure in Sec. II. Section III will present the experimental data and discuss on the different parameters influencing flow properties. Section IV will examine various theoretical models developed to model granular flows in a frictional-collisional regime. Their predictions will be compared with our data.

II. EXPERIMENTAL SETUP AND PROCEDURES

A. Experimental device

As illustrated in Fig. 2, the experimental setup consisted of a 2-m-long channel, two hoppers, and a pumping system. The base of the channel was roughened by gluing beads on a thin PVC band. After testing various glues, we found that the best technique involved depositing beads on a double-sided adhesive film. In this way a uniform random distribution of beads over the surface was achieved. We made different kinds of roughness. The typical diameter of roughness (r) ranged from 0.36 to 2 mm. At the upper channel entrance, the supply hopper fed the channel through an intermediate chamber. The mass flow rate was controlled by either a sluice gate at the exit of the chamber or directly at a cone-shaped valve, which more or less obstructed the hopper exit. In most cases, the latter system was used because it enabled us to obtain very large mass flow rates. The material flowed down the channel and fell into a collection hopper. Screws powered by two Siemens gears returned the material to the supply hopper. The maximum mass flow rate was 1.5 kg/s. The cone-shaped valve was calibrated by weighing the mass of fallen material for a given time interval. As is well known for bins and hoppers, the mass flow rate does not depend on the height of material stocked inside the hopper, but only on the exit geometry [34]. Uncertainty on the mass flow rate was estimated around 5%. Tests were also performed to verify whether vibrations induced by the two gears could affect the mass flow rate. Within the range of uncertainty, no vibration-induced effect was detected.

The channel inclination ranged from 0 ° to 38 °. It was measured using an electronic clinometer PRO 360 provided by the company PM Instrumentation. According to the provider, slope uncertainty was approximately 0.1 °, but due to the channel flexing as a result of its own weight, variations of about 0.1 ° were possible at the middle of the channel. We maintained an uncertainty of less than 1%. Two types of channel were used. The first one was 2.5 cm wide and built in PVC. The second one was 4.8 cm wide and primarily designed in Plexiglas to have transparent sidewalls. However, to avoid strong electrostatic effects produced by the flowing material, the sidewalls had to be covered with an antielectrostatic film.

Flow depth was measured using electronic ultrasonic sensors LRS3 provided by Weidmüller (Germany). This sensor sent an ultrasonic wave, then measured the time necessary for the wave to return by reflection against the free surface, and finally computed the distance separating it from the free surface. Due to the width of the spot, the flow depth was averaged on a surface of 18 cm^2. Four or six ultrasonic sensors were connected to a computer via a data acquisition device operating at a sampling rate of 100 Hz. Signals emitted by sensors were collected, filtered, and averaged over a given time interval (generally 10 s). Uncertainty in the measurements was normally less than 0.1 mm according to the manufacturer, but due to various disturbing effects (saltation of particles, roughness of the free surface, air motion due to the large velocity at the free surface), we found that the uncertainty was much greater, close to 1 mm for the coarsest particles. For 2-mm glass beads, uncertainty on the flow depth was as high as 10% while it did not exceed a few percent for small particles. Velocity profiles at the sidewalls and the free surface were measured using a video camera (Pulnix progressive scan TM-6705AN coupled to an acqui-

TABLE I. Main features of particles.

Material	Composition	ρ_p(kg/m^3)	d (mm)	Grain size distribution	φ (°)
Material 1	Glass	2460	0.36	Poorly sorted	26.5
Material 2	Glass	2460	0.97	Poorly sorted	26.5
Material 3	Glass	2460	2.0	Well calibrated	26.5
Material 4	Glass	2460	3.0	Well calibrated	26.5
Material 5	Sand	2650	0.33	Poorly sorted	36.0

sition card, Meteor II MC, provided by Matrox) and an image processing system (WIMA software provided by the University of Saint-Etienne, France). Pictures were acquired at a rate of 208 frames/s. Even though particles glided along the sidewalls, it turned out that the velocity underwent a significant decrease near the walls. The thickness of the disturbed zone was estimated at five layers of particles. When we compared the free-surface velocity at the sidewall and at the centerline, we found that the relative decrease ranged from 30% to 50%. Moreover, as velocities at the free-surface were at times very large (exceeding 1 m/s), uncertainty could be significant in the upper part of the velocity profile and indeed exceeded 10%, while it was less than 6% close to the channel base. Measuring the velocity profiles at the sidewall was expected to provide only qualitative information. Because of these severe limitations, we did not try to measure the temperature profiles, which would have been even more influenced by the sidewalls.

Density profiles were measured using γ-radiation techniques. These techniques involve measuring the quantity of γ photons emitted by a radioactive source that is absorbed by a material of density ρ and thickness W [36]. The density can then be computed as: $\rho W = -K \ln(I/I_0)/\mu'$, where I_0 denotes the intensity of γ photons emitted by the radioactive source, I the measured intensity of photons after crossing the material, μ' the absorption coefficient (per unit mass), K a fitting parameter depending on the apparatus. We used a Cesium

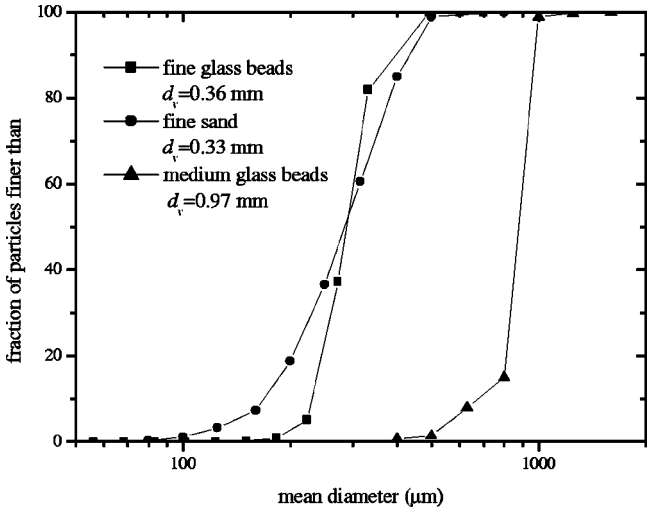

FIG. 3. Volume or mass size distribution of the poorly sorted materials.

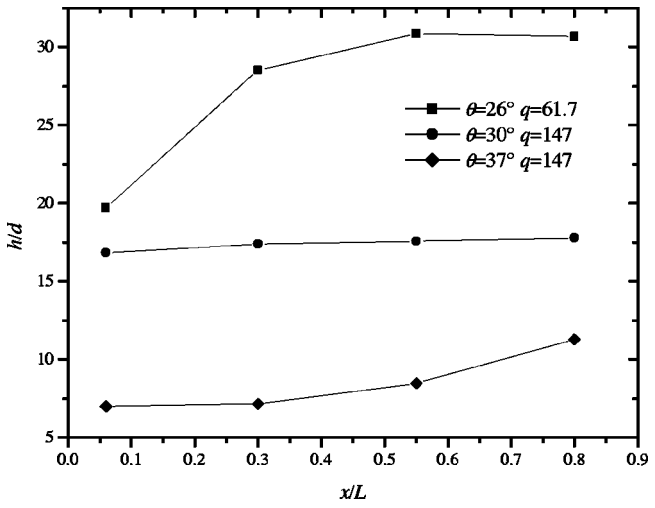

FIG. 4. Variation of the dimensionless flow depth as a function of the distance from the channel exit (scaled by the channel length) for three different slopes and dimensionless flow rates. The channel width was 4.8 cm.

137 source, which operated with an activity of about 7 mCi. The signal was collected by a receiving system made up of a scintillation crystal (NaI activated by thallium) with a photomultiplier. The channel was located between the emitting and receiving systems. Measurements were performed at different points across the flow depth. Uncertainty on the density was less than 4%.

B. Materials

For our tests, we used different kinds of glass beads and fine sand. The mean diameter d ranged from 0.36 mm to 2 mm. The main characteristics of these materials are reported in Table I. Apart from beads 2 mm in diameter, the material was poorly sorted with a gradation in size. For 2-mm glass beads, the manufacturer's tolerance on the diameter was 10%. In Fig. 3, we give the size distribution of the finest glass beads, which was determined using a laser device designed by Malvern. We also determined the internal friction

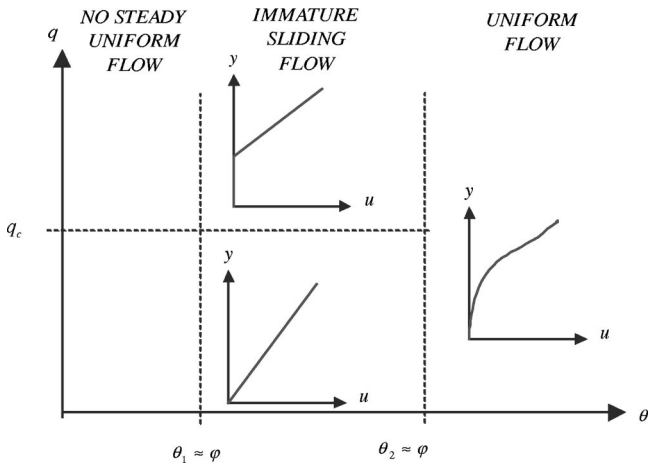

FIG. 5. Schematic diagram delineating the different regimes depending on the channel slope and flow rate.

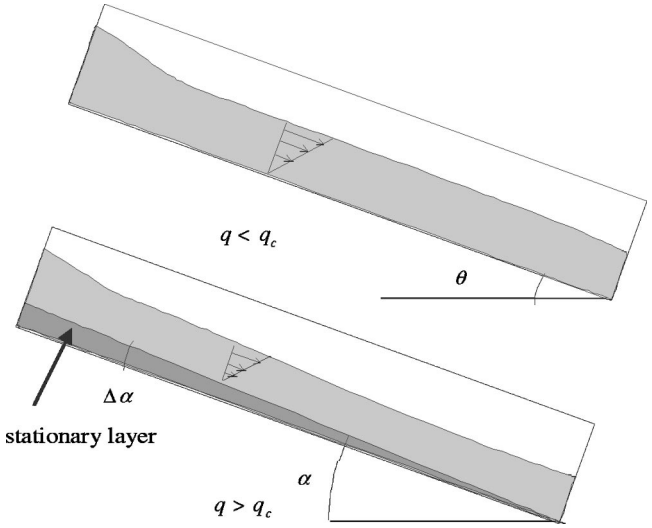

FIG. 6. Development of a stationary wedge when the channel slope is lower than a critical value θ_1 and the discharge exceeds a critical value.

angle of the materials by using soil-mechanics techniques (triaxial). Uncertainty on the internal friction angle was $\pm 0.5°$. Abrasion occurred due to significant friction inside the recirculation system, but this did not cause a significant change in the material properties (sphericity, internal friction angle) during our tests.

C. Experimental procedure

The following experimental procedure was used. We selected a channel-base roughness. The four (or six) ultrasonic sensors were initialized. For a given channel inclination, we imposed a mass flow rate by rotating the cone-shaped valve of the supply hopper. We recorded the signals of flow depth measurement given by ultrasonic sensors at four or six different locations. As with a typical flow depth, we kept the value(s) measured in the region where the flow reached a uniform depth. Figure 4 shows different streamwise profiles of the flow depth for different slopes. It can be seen that the region where a uniform flow depth was reached in a steady regime could occupy a limited part of the channel length. For instance, at low and high slopes, this part represented 20% of the total length while for an intermediate slope ($30°$) the flow was uniform over almost the entire length.

III. EXPERIMENTAL DATA AND DISCUSSIONS

The observed behavior was quite complex and is, probably, best explained by first describing the typical flow pattern, then by examining each regime of this overall pattern, indicating the common points in the behavior observed for various materials and the diverging points as well. In the following, we use dimensionless parameters: $q_* = q/(d\sqrt{gd})$, $h_* = h/d$, $u_* = u/\sqrt{gd}$, with g the gravity acceleration. The mean velocity was computed as: $U = q/h$ ($U_* = q_*/h_*$). The discharge q per unit width was deduced from the mass flow rate per unit width q_m by assuming that the density was nearly uniform for a steady flow: $q_m = \overline{\phi}\rho_p q$, with $\overline{\phi} = 0.6$. This was obviously quite a crude assumption since it was experimentally found that bulk density ranged from 0.47 to 0.58 and could be as low as 0.38 for dilute flows on high slopes. At this stage, it is also worth mentioning that in the scaling of the flow rate, we did not take the channel width into account. Given the narrow channel and the sidewall effects, we expected the width to influence the discharge. Such an effect is well known in hydraulics, where for narrow, straight, smooth, rectangular channels, it has been shown that the total flow rate scales as $Wh^{5/3}$ for shallow flows but as $(Wh)^{5/3}$ for thick flows [35]. Even in this simple case (Newtonian fluids and uniform roughness), it is far from easy to include the width effect directly in the scaling of the flow rate by using a single expression. This explains why here we prefer not to include W in the scaling of q.

A. Flow regimes: Qualitative observations

Experimentally it was observed that three parameters played a key role in the granular flow dynamics: first the channel inclination and to a lesser extent the discharge and the kind of roughness. On the whole, we found that, qualita-

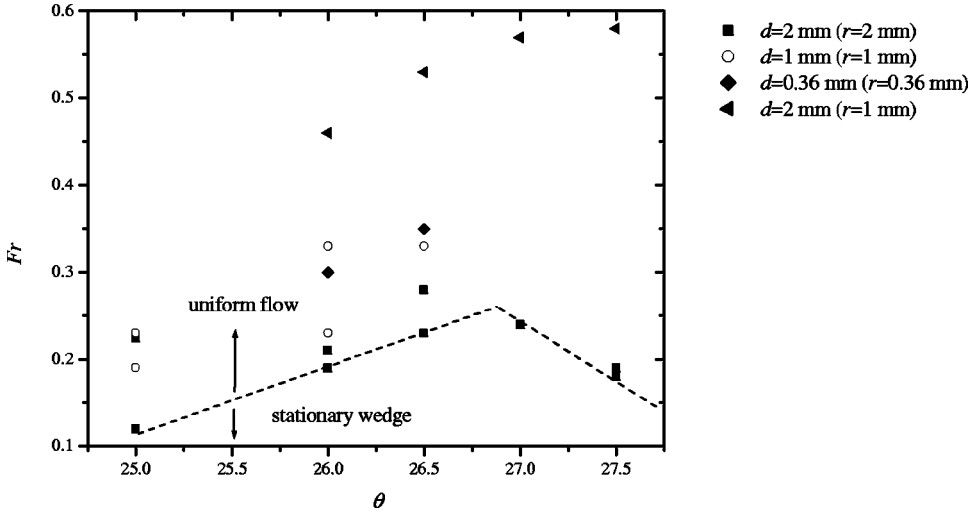

FIG. 7. Estimation of critical Froude number below which a stationary wedge develops along the channel bottom.

tively, our observed flow pattern was similar to that described by Savage [1] even though differences were detected (mainly because we investigated flow properties over a wider range of flow rates). In the following, we will use his terminology to refer to the different regimes (see Fig. 5).

For a steady uniform flow to occur, the channel inclination must be in excess of a critical value θ_1 (approximately 24° for glass beads). For a slope ranging from θ_1 to another critical value θ_2, very close to the internal friction angle of the material φ (26.5° for glass beads), a steady uniform flow was possible, but it was stable only for a narrow range of the mass flow rate. For large mass flow rates, a stationary wedge-shaped layer developed along the channel bottom and induced a change in the bottom slope over which the granular material flowed (see Fig. 6). Flows of this regime have been called ''immature sliding flows.'' As the stationary wedge could be observed only at the channel sidewalls, we wondered whether it spanned across the channel or was localized at the corners. The former interpretation appeared to us as the more probable, since when we stopped supplying the material, we observed a stationary wedge covering the channel bottom and not a string of particles trapped along the corners. We also measured the inclination α (to the horizontal) of the boundary separating the flowing material from the stationary material at the sidewall. On the whole, the angle α depended a great deal on the roughness type as well as the initial channel slope, and to a lesser extent on the flow rate. For instance, the dead zone formation was achieved at substantially higher discharges when reducing the roughness size (see Fig. 7). Moreover, the angle α barely exceeded the internal friction angle. In the case of 2-mm glass bead flows along a bottom made up of the same material, for example, $\Delta\alpha=\alpha-\phi$ ranged from 0.9° to 1.9°. We failed to find a reproducible close correspondence between the value of α and flow conditions. Even in determining the flow conditions for which a stationary wedge developed, we were faced with widely distributed data scattering: in Fig. 7, we have reported the critical Froude number separating flows without and with a stationary wedge. The critical Froude number was estimated as $\mathrm{Fr}=U/\sqrt{gh}=U_*^{3/2}q_*^{-1/2}$, where (U,h) corresponded to the limiting flow conditions for which a uniform flow was observable. From one experiment to another, this Froude number could vary significantly. For instance, for 2-mm glass beads flowing down a channel inclined at 25°, the critical Froude number ranged from 0.12 to 0.22. The characteristic time associated with the formation of the stationary zone was long, typically between 40 s and 60 s for our tests. Observations at the sidewalls revealed that the velocity profile was almost linear and the density was nearly uniform close to the bottom but decreased significantly near the free surface.

For slopes ranging from θ_2 to another critical value θ_3 (approximately 34°–35° for glass beads), a steady uniform flow occurred. Such a regime has been called a ''fully developed steady regime.'' The flow density was rather uniform throughout the flow depth except near the free surface. Inside the slope range $[\theta_2,\theta_3]$, various types of flow were possible depending on the flow rate (see below). Generally we observed that at low discharge, particles reached a large velocity and the flow was thin. Conversely, for a large discharge, the flow was much thicker and particles moved more slowly. For slopes in excess of the third critical value θ_3, which depended on the discharge, the particles of the upper layers were increasingly agitated with increasing discharge or slope. They were no longer in close contact but in saltation and thus the accurate position of the free surface was hard to measure. Such a regime has been called a ''splashing regime.''

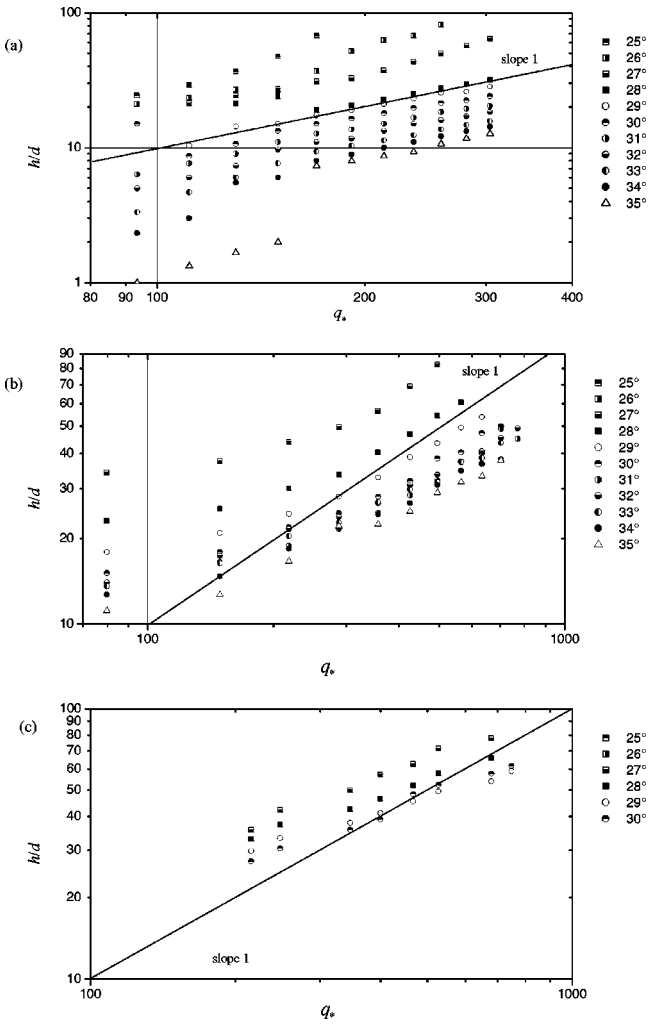

FIG. 8. Discharge curves (dimensionless flow depth h_* versus dimensionless mass flow rate q_*) for 0.36-mm glass beads flowing. (a) $W=25$ mm and $r=0.36$ mm. (b) $W=48$ mm and $r=0.36$ mm. (c) $W=48$ mm and $r=1$ mm.

B. Discharge curves

All the raw data are presented in Figs. 8–14. For each material and roughness, we have reported the discharge curves and the variations in the mean velocity as a function of the flow rate and slope. In order to identify flow regimes, we have reported experimental points in dimensionless log-log plots and we tried to fit them with power functions: $q_* \propto h_*^n$ and $U_* \propto q_*^m$ (normally we should obtain $m=1-n^{-1}$ since $U_*=q_*/h_*$). This was usually achieved using the least-squares method on parts of the experimental curves.

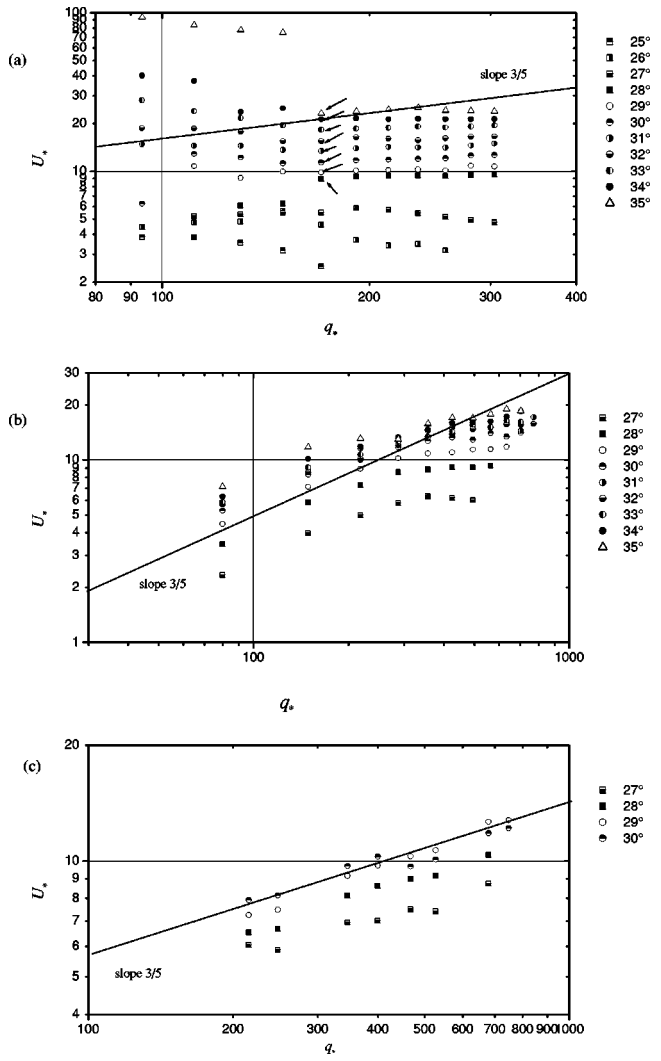

FIG. 9. Variation in the dimensionless mean velocity U_* as a function of the dimensionless mass flow rate q_* for 0.36-mm glass beads flowing. (a) $W=25$ mm and $r=0.36$ mm; the arrows indicate the data used for Fig. 16 (transition from regime *A* to regime *B*). (b) $W=48$ mm and $r=0.36$ mm. (c) $W=48$ mm and $r=1$ mm.

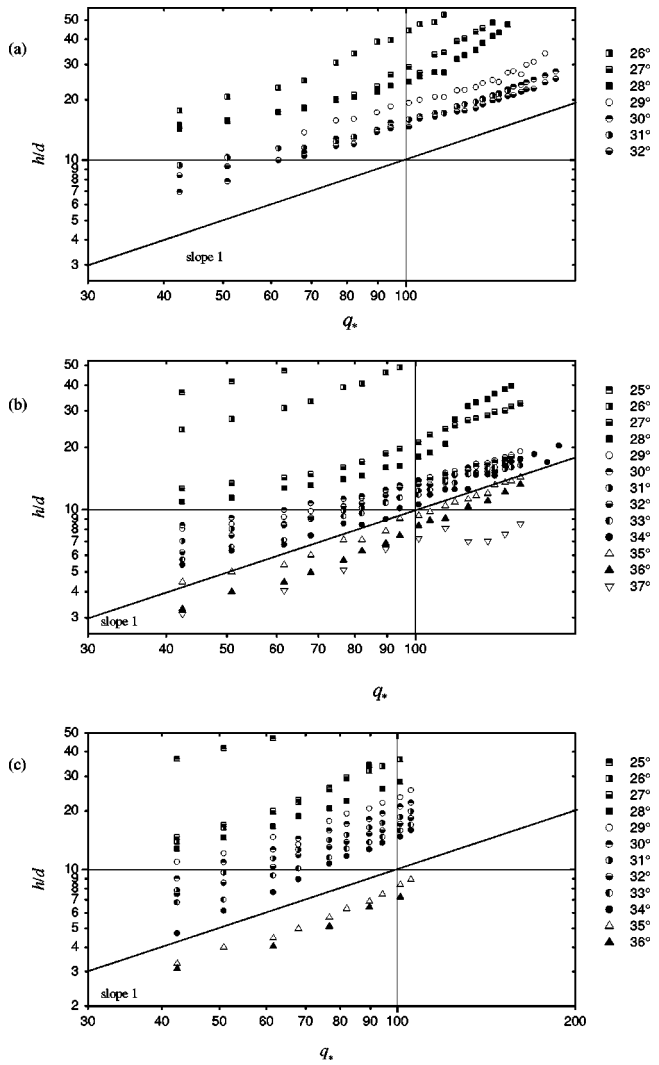

FIG. 10. Discharge curves for 1-mm glass beads flowing. (a) $W=48$ mm and $r=1$ mm. (b) $W=48$ mm and $r=0.36$ mm. (c) $W=48$ mm and $r=2$ mm.

Figures 8 and 9 express the variations in the dimensionless flow depth and the mean velocity with respect to the flow rate for 0.36-mm glass beads. Figures 8(a) and 9(a) include the experimental data obtained with a roughness of 0.36-mm glass beads and a 25-mm channel width while Figs. 8(b), 8(c), 9(b), and 9(c) include the data obtained with the wide channel and different degrees of roughness. As stated above, a noticeable feature is the change in behavior when the channel slope passes from 26° to 28°, i.e., θ is close to the internal friction angle φ. Such an effect is particularly obvious for mean velocities [see Fig. 9(a)]: when the channel slope was increased from 27° to 28°, the mean velocity was doubled at high discharges. For $\theta \leqslant 27°$, we have reported data pertaining to a fully uniform flow (i.e., we discarded data associated with the development of a stationary layer at the bottom). Surprisingly enough, for such a domain of slopes, the mean velocity first increased, reached a maximum, then decreased for increasing flow rates: the lower the slope, the greater the rate of decay. On the whole, small changes in the slope induced substantial changes in the mean velocities. For $\theta \geqslant 28°$, there were two types of behavior depending on the flow rate. For $q_* \geqslant 170$, the flow depth increased almost linearly with the flow rate ($n \approx 1$), which implies that the mean flow velocity was fairly constant, as shown in Fig. 9(a). The influence of the channel slope was regular. In contrast, for $q_* < 170$, the behavior was much more complex. When fitting the mean velocity with power functions q_*^m, we found that $m \approx 1$ for $\theta = 28°$, $m \approx 0$ on average for θ in the range $29° - 31°$, and $m \approx -1$ for $\theta > 32°$. Moreover, the transition from lower to higher discharges was generally continuous, but in some cases [$\theta = 28°$ and $\theta = 35°$ in Fig. 9(a)], there was an abrupt jump at $q_* = 170$.

Similar experiments were performed with a 48-mm-wide channel and a 0.36-mm roughness [see Figs. 8(b) and 9(b)]. On the whole, the flow pattern was close to that observed with the narrow channel. At low discharges ($q_* \leqslant q_{c*} \approx 275$–$290$), velocities varied as q_*^m with m, ranging

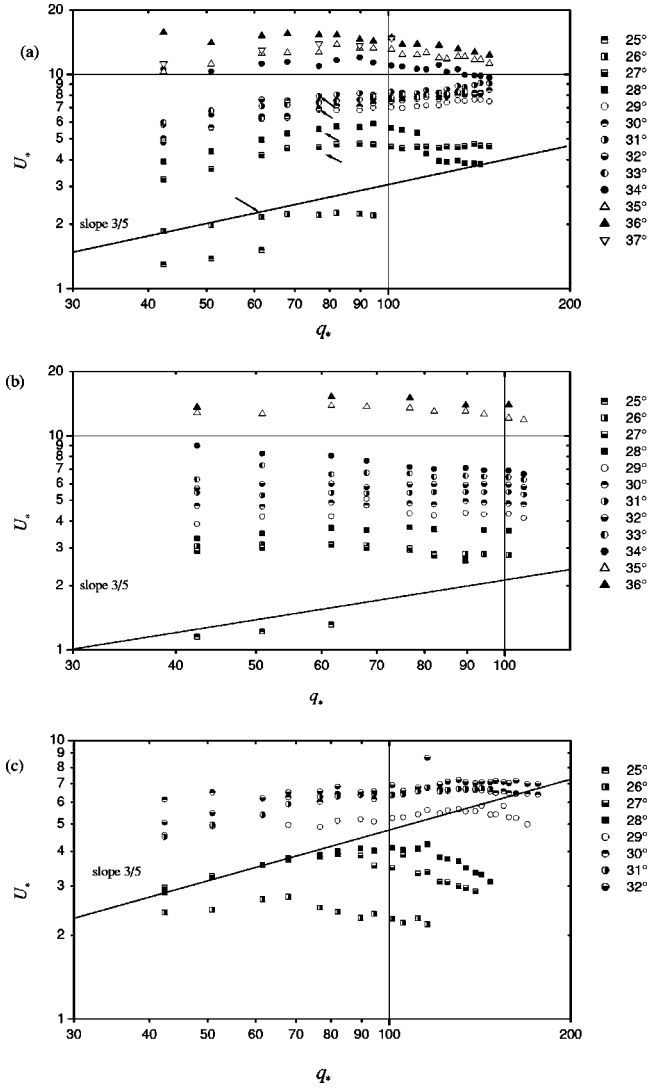

FIG. 11. Variation in the dimensionless mean velocity U_* as a function of the dimensionless mass flow rate q_* for 1-mm glass beads flowing. (a) $W=48$ mm and $r=1$ mm; the arrows indicate the data used for Fig. 16 (transition from regime A to regime B). (b) $W=48$ mm and $r=0.36$ mm. (c) $W=48$ mm and $r=2$ mm.

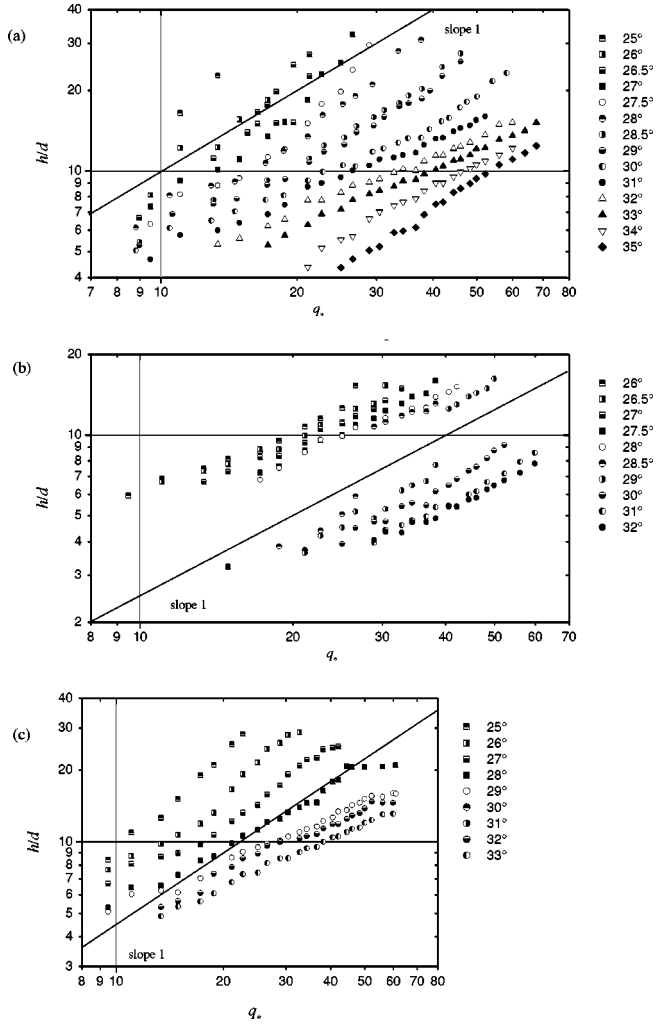

FIG. 12. Discharge curves for 2-mm glass beads flowing. (a) $W=48$ mm and $r=2$ mm. (b) $W=48$ mm and $r=0.36$ mm. (c) $W=48$ mm and $r=1$ mm.

from 0.51 to 0.66 (mean computed value: 0.59). For the largest slopes ($\theta \geqslant 34°$), this trend was less obvious due to data scattering. At high discharges, the velocities reached a seemingly constant value. This trend was less evident than for the former case ($W=25$ mm) since here the critical flow rate was too close to the maximum achievable flow rate. Compared to data obtained with the narrow channel, velocities were slightly lower: the relative difference usually did not exceed 5%, except for largest slopes ($\theta \geqslant 34°$) for which it reached 20%. Nevertheless, the critical flow rate around which flow passed from the first regime ($U_* \propto q_*^m$, $\neq 0$) to another one ($U_* \approx cst$) was significantly higher: with the wide channel, we found $q_{c*} \approx 275$–290 for $\theta < 34°$ and $q_{c*} \approx 420$–430 for $\theta \geqslant 34°$ while we found $q_{c*} \approx 150$–170 for the narrow channel. The ratio between the two critical values (approx 1.7) was close to the width ratio (1.9).

Another set of experiments was performed with the broad channel equipped with the 1-mm roughness [see Figs. 8(c) and 9(c)]. For this configuration, the flow pattern differed from the two previous ones in that we did not observe the asymptotic regime $U_* \approx cst$. The mean velocities varied as q_*^m with m, ranging from 0.33 to 0.45. As the channel was rougher for this set of experiments, a lower mean velocity was expected. This was experimentally checked except for lower slopes. Strikingly, at $\theta=27°$, the mean velocity was 20% higher than for the smoother channel.

Figures 10 and 11 include all the data obtained with 1-mm glass beads. On the whole, when they flowed over a 1-mm rough bottom, these beads exhibited the same flow pattern as for 0.36-mm glass beads [see Figs. 10(a) and 11(a)], namely, a q_*^m variation in the mean velocity at low discharges, a fairly linear discharge curve at large flow rates ($n \approx 1$), and sudden changes in bulk behavior for slopes close to the internal friction angle and for slopes exceeding 34°. Closely examining the experimental curves revealed other interesting features. First, the ''asymptotic'' regime at large discharges was less marked than for 0.36-mm glass beads. When using the least-squares method to fit data at large discharges, we found that the mean velocity scaled as q_*^m with $m \approx 0.04$–0.06 for θ

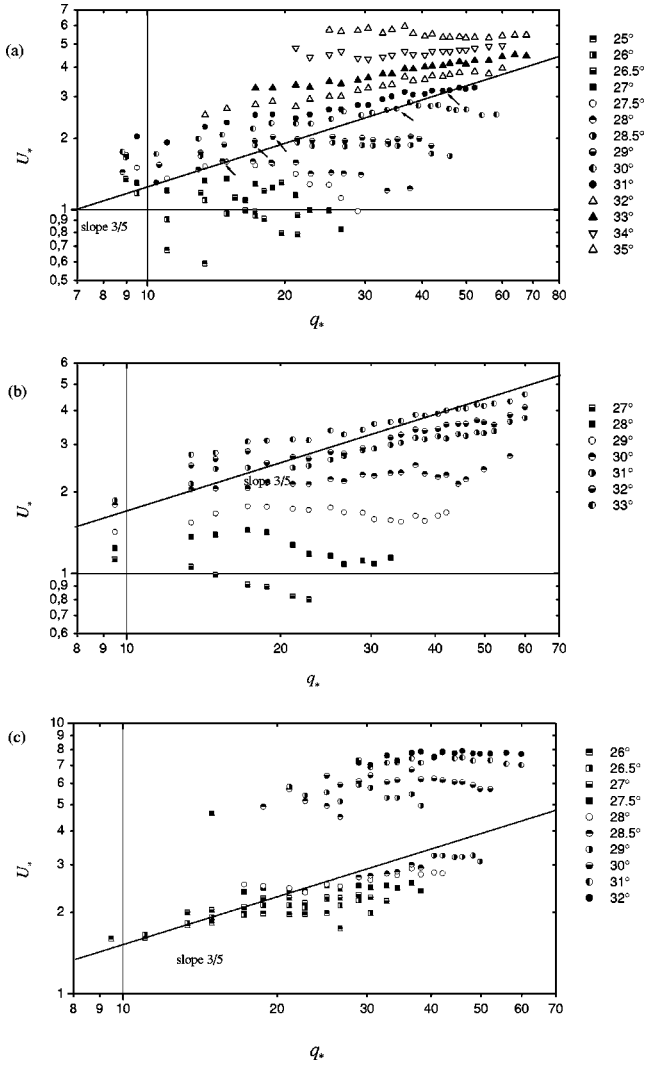

FIG. 13. Variation in the dimensionless mean velocity U_* as a function of the dimensionless mass flow rate q_* for 2-mm glass beads flowing. (a) $W=48$ mm and $r=2$ mm; the arrows indicate the data used for Fig. 16 (transition from regime *A* to regime *B*). (b) $W=48$ mm and $r=0.36$ mm. (c) $W=48$ mm and $r=1$ mm.

$\leqslant 28°$ while we obtained $m=0.14\pm0.04$ for $29°\leqslant\theta\leqslant33°$. For the largest slopes ($\theta\geqslant34°$), the exponent m was negative: $-0.29\leqslant m\leqslant-0.15$. Second, at low flow rates, the mean velocity varied as q_*^m with $m\approx0.33$ for $\theta\leqslant26°$ but $m=0.57\pm0.1$ for $27°\leqslant\theta\leqslant33°$. For large slopes ($\theta\geqslant34°$), the discharge curve seemed to be almost linear over the range of flow rates 40–80 but the fluctuations were too high for a sharp trend to be revealed. Third, when examining Figs. 10(a) and 11(a), we found two critical values of the dimensionless flow rate, for which there was a change in the flow behavior. In the vicinity of $q_{c*}\approx68-84$, there was a systematic but continuous decrease in the exponent of the discharge equations, e.g., from 0.57 to 0.14 for slopes ranging from 27° to 33°. Another seemingly critical value was revealed by the peculiar behavior of the 28° and 37° discharge curves at $q_{c*}\approx110$. For these two inclinations, there was a sudden and odd change in the discharge curves, which either decreased or increased abruptly. Fourth, in contrast to

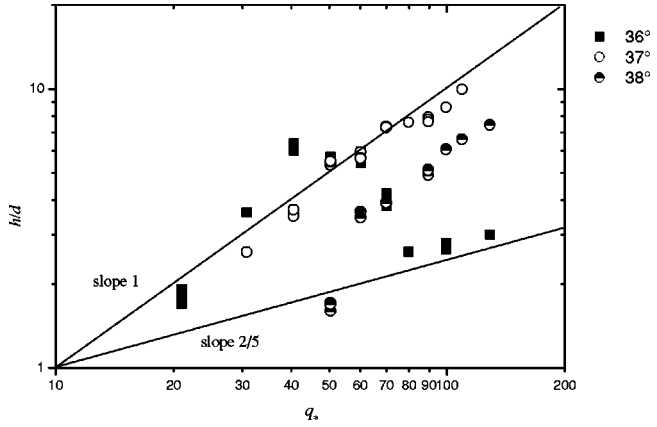

FIG. 14. Discharge curves for sand.

0.36-mm glass beads for which 28° was the critical slope around which significant changes in bulk behavior were observed, here we found that such changes occurred between 26° and 27°.

Similar experiments were performed with different roughnesses. When the roughness was made up of 0.36-mm glass beads, the separation into two regimes was more distinct [see Figs. 10 and 11(b)]. Indeed, for flow rates in excess of a critical value around 70, we observed an asymptotic regime for which the discharge curve was linear, implying that the mean velocity was constant. For flow rates lower than 70, the mean velocities varied as a power function of the flow rate: $U_*\propto q_*^m$. The exponent m depended on the slope as shown in Fig. 11(b): we found $m\approx0.35$ for $\theta\leqslant28°$, $0.01<m<0.05$ for $29°\leqslant\theta\leqslant33°$, and $-0.32<m<-0.06$ for $34°\leqslant\theta$. When the roughness was made up of 2-mm glass beads [see Figs. 10(c) and 11(c)], we still observed two regimes depending on whether the flow rate was in excess of a critical value close to 70. At low discharges, the mean velocity was an increasing function of the flow rate: $U_*\propto q_*^m$ with $m=0.48\pm0.09$. In contrast, at high discharges, the mean velocity was a decreasing function, with an exponent taking a value close to -0.6 for slopes lower than 28° and close to -0.03 for $\theta\geqslant29°$. Contrary to previous experiments, the critical flow rate associated with this change in behavior was not constant but increased with the slope, from 70 for $\theta=26°$ to 120 for $\theta\geqslant29°$.

Figures 12 and 13 summarize the experimental data concerning 2-mm glass beads and different roughnesses. Figures 12(a) and 13(a) report the data obtained with a 2-mm roughness. Even though bulk behavior presented features common to those observed with finer materials, it differed significantly on many points. For slopes $\theta\leqslant28°$, large fluctuations in the flow depth induced a significant data scattering. As reported for $\theta=26.5°$, the mean velocity varied in the range 0.6–1.3, without a clear trend being outlined. The mean velocity curve first increased, then flattened out over a fairly wide range of flow rates, and finally decreased slowly. For $29°\leqslant\theta\leqslant33°$, two regimes were identified depending on the discharge. At low discharges, the mean velocity rose as $U_*\propto q_*^m$. The exponent m was a decreasing function of the slope: the least-squares method gave $m\approx0.6$ for $\theta=29°$

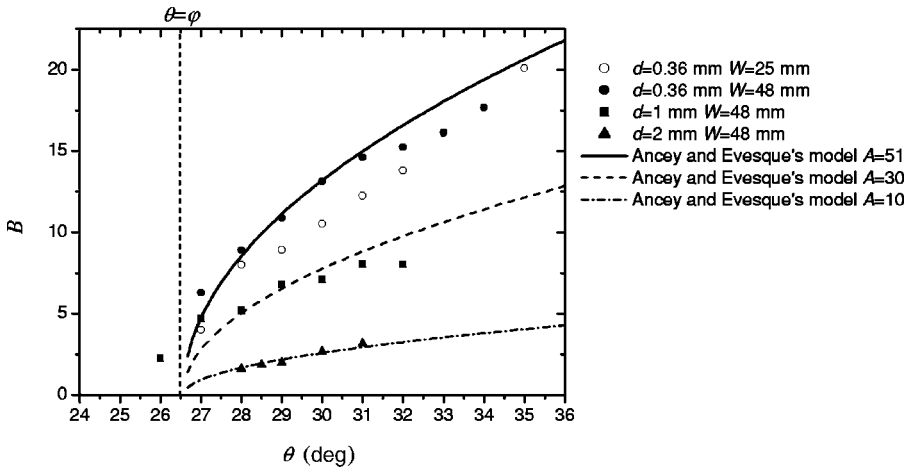

FIG. 15. Variation in the coefficient B as a function of the slope in regime A. Experimental data were taken from Figs. 9(a), 11(a), and 13(a).

against $m \approx 0.28$ for $\theta = 33°$. At large discharges, the mean velocity increased more slowly with the flow rate since the exponent m was found close to 0.2 ± 0.1. For $\theta \geqslant 34°$, a single regime could be identified within the range of tested flow rates. As for $29° \leqslant \theta \leqslant 33°$, we found that m was a decreasing function of the slope, varying from 0.28 for $\theta = 33°$ to -0.09 for $\theta = 35°$. When a 0.36-mm roughness was used instead of a 2-mm roughness [see Figs. 12(b) and 13(b)], we observed small changes. Surprisingly, however, when we used a 1-mm roughness [see Figs. 12(c) and 13(c)], more substantial changes occurred. On the whole, for $\theta \geqslant 27°$, the velocities were constant over the range of tested flow rates. A striking feature was that rather systematically at low discharges for $\theta \geqslant 27.5°$, the mean velocities were much higher compared to those measured with the two other degrees of roughness: indeed, for $q_* = 30$, the dimensionless velocities ranged from 5 to 8 whereas they did not exceed 5 for 2-mm and 0.36-mm roughnesses. Another interesting feature was that these velocities corresponding to shallow flows of vigorously agitated particles decreased abruptly or, in other words, flows thickened suddenly at a given critical discharge q_{c*}. This can be seen in Fig. 12(c) for $\theta = 27.5°$ at $q_{c*} \approx 15$, $\theta = 28.5°$ at $q_{c*} \approx 27$, and $\theta = 29°$ at $q_{c*} \approx 39$.

Figure 14 reports the data obtained with fine sand. Compared to glass beads, fluctuations in the flow depth signal were much more significant. Moreover, due to the high value of the internal friction angle, experiments could be performed over a tight range of slopes. Nevertheless, it was observed that for slopes in excess of the internal friction angle and for sufficiently higher discharges, the discharge curve was approximately linear.

In summary, when comparing the various experimental trends appearing in Figs. 8 –14 with bulk behaviors usually exhibited by various other complex fluids (suspension, pastes, etc.), the most striking feature is the great variability of the discharge curves with respect to the particle diameter, the roughness size, and the channel slope. Any attempt to classify fully developed flows is rendered difficult by this sensitivity of the experimental data to even small changes in the control parameters (slope, roughness) and the number of effects to take into account. A crude classification of the discharge curves could be the following. For an inclined channel, whose roughness is made up of particles with the same diameter as the flowing particles, there are two regimes. The first regime, which we call ''regime *A*,'' occurs at low discharges and is characterized by an equation in the form $U_* = A(\theta) q_*^m$, with m ranging from 0.66 to 0.33 [or, equivalently, $q_* = A^n(\theta) h_*^n$, with n in the range $2-3$]. The second regime, referred to as ''regime *B*,'' occurs at high discharges and it is characterized by a fairly linear discharge curve since the flow depth varies as $q_* = B^n(\theta) h_*^n$, with n

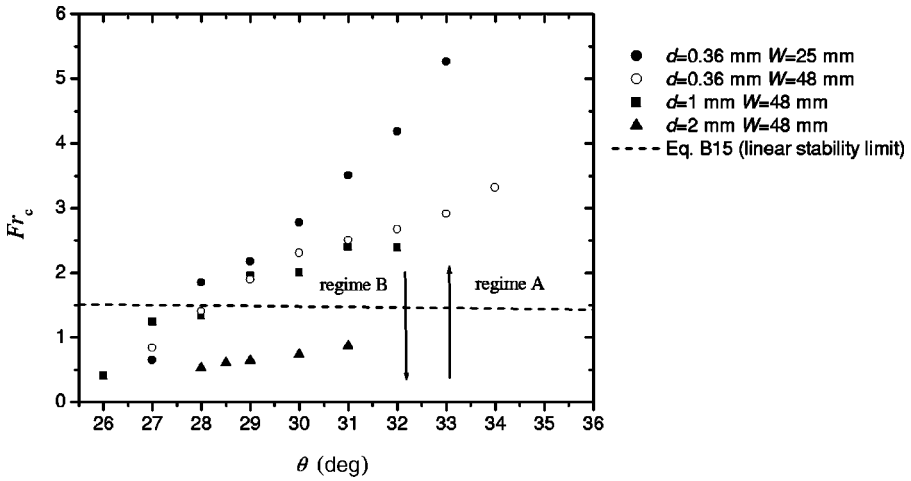

FIG. 16. Plot of the critical Froude number (transition from regimes A to B) vs channel slope. The dashed curve represents the limits of linear stability given by Mills *et al.*'s model. The arrows indicate that when the flow rate is increased progressively from zero, first regime *A* occurs (leading to an increase in the Froude number), then, after the critical value has been reached, regime *B* occurs (leading to a decrease in the Froude number).

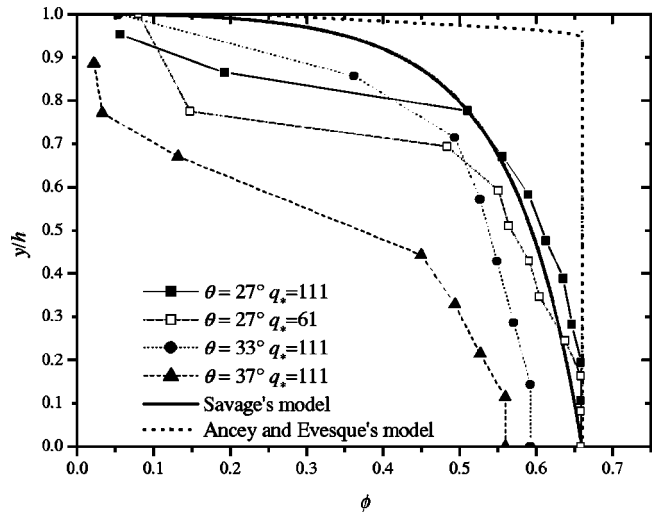

FIG. 17. Dimensionless density profiles for 1-mm glass beads flowing down a 48-mm-wide channel at three different slopes and for mass flow rate of 430 g/s ($q_*=61$) or 784 g/s ($q_*=111$). For $\theta=27°$, $h=15$ ($q_*=61$) or $h=26$ mm ($q_*=111$), $\theta=33°$ $h=14$ mm, for $\theta=37°$ $h=8.1$ mm. The continuous lines represent the theoretical profile provided by Savage's model and Ancey and Evesque's model.

ranging from 0.97 to 1.16 [or, equivalently, $U_*=B(\theta)q_*^m$, with m ranging from -0.03 to 0.14]. Figures 9(b) and 11(a) give typical examples of these regimes. However, such a pattern holds partially for 0.36-mm glass beads in a narrow channel [see Fig. 9(a)] and 2-mm glass beads [see Fig. 13(a)]. In Fig. 15, we have reported the variation of the coefficient B as a function of the slope. It can be seen that the coefficient is a function of the slope, rapidly increasing for slopes just in excess of the internal friction angle, then growing more slowly for 0.36-mm and 1-mm beads in the wide channel. Coefficient B decreases with increasing particle diameter d. In spite of the low number of points, we fitted a power function to describe the variation in B with d. We found $B(\theta)\propto d^{-0.97\pm0.02}$. Another interesting point is the transition from regime A to regime B. From a physical viewpoint, it is more convenient to describe this transition in terms of a dimensionless number. We used the Froude number since it is encountered in most transitions concerning gravity-driven free-surface flows. Figure 16 reports the variation of the critical Froude number as a function of the slope in the case of glass beads flowing down a channel whose roughness size was the same as the flowing bead diameter. Data used for this figure originate from Figs. 9(a) and 9(b), 11(a), and 13(a) (data marked with an arrow). The critical Froude number was reached but not exceeded. Indeed, when flow was generated with a small flow depth (namely, in regime A), the Froude number rose as $\mathrm{Fr}\propto H^p$, with p close to 1, as the flow depth was increased. When the critical Froude number was reached, there was a transition from regime A to regime B. For regime B, the Froude number decreased as $\mathrm{Fr}\propto 1/\sqrt{H}$ as the flow depth was increased. For 1-mm and 0.36-mm glass beads in the wide channel, the critical Froude number curves were very close. Decreasing the channel width provoked an increase in the value of the critical Froude number for slopes in excess of 30°, as can be seen in Fig. 16 for 0.36-mm glass beads. Data corresponding to 2-mm glass beads are far below the experimental curves associated with 1-mm and 0.36-mm glass beads.

For a rougher channel bottom, two regimes were identified. The first regime presents features similar to regime A above, namely, the coefficient n in the discharge equation ranged from 1.85 to 3. At high discharges, the mean velocity curve either flattened out or decreased: the exponent m ranged from -0.58 to -0.03 for 1-mm glass beads [see Fig. 11(c)] while it ranged from 0.16 to 0.29 for 0.36-mm glass beads flowing down a 1-mm roughness [see Fig. 9(c)]. For a smoother channel base, the discharge curve was rather flat [see Fig. 13(c) for 2-mm glass beads down a 0.36-mm roughness and Fig. 11(b) for 1-mm glass beads flowing down a 0.36-mm roughness].

C. Density and velocity profiles

Figure 17 expresses the typical variation of the solid fraction profile across the depth for three slopes (27°, 33°, 37°). In each case, the solid fraction was a decreasing function of the flow depth. It was close to the maximum random solid concentration at the channel bottom, then tended towards zero close to the free surface. Depending on the channel slope, the decrease was more or less regular. For low slopes (typically 27° in Fig. 17), for a dimensionless flow depth up to 0.8, the solid concentration varied slightly in the range 0.55–0.65. Conversely, for high slopes (37°), the solid concentration decreased rapidly. The flow rate had little influence on the density profile. For instance, for $\theta=27°$, doubling the flow rate (namely, passing from regime A to B) did not alter the profile form but led to a larger mean bulk density (0.55 instead of 0.47). For the same flow conditions as in Fig. 17, Fig. 18 reports the velocity profile in a dimensionless form. The velocity has been scaled by the velocity at the free surface u_l and the thickness from the bed y by the flow depth h. Contrary to density profiles, which represent width-averaged values, the velocity profiles were measured at the sidewalls and thus were strongly disturbed. For instance, the mean velocities computed from the experimental velocity profiles in Fig. 18 were approximately half the mean velocity $U=q/h$. However, despite this significant disturbing effect, it is expected that the experimental velocity profiles can provide a good idea of the actual velocity profiles within the flowing materials; moreover, using scaled variables should offset the influence of sidewalls. In regime A ($\theta=27°$ in Fig. 18), the velocity profile was fairly linear while in regime B, it was convex except near the free surface. An inflection point could be identified at approximately $y/h\approx0.8$. A striking feature was that the velocity profile on large slopes was very similar to the typical velocity profile measured at $\theta=33°$ although velocities were much higher.

IV. COMPARISON WITH THEORETICAL MODELS

A. Theoretical models

To our knowledge, the earliest model suitable to describing granular flows in a frictional-collisional regime down an

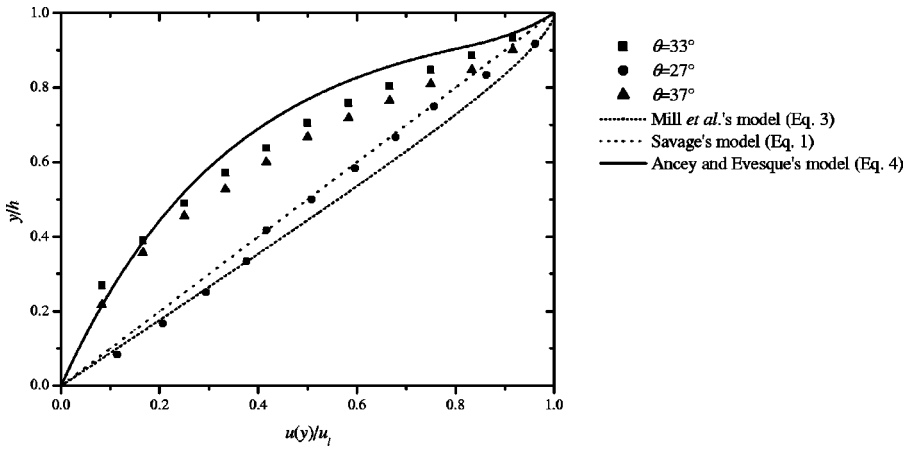

FIG. 18. Dimensionless velocity profiles for 1-mm glass beads flowing down a 48-mm-wide channel at three different slopes and for various mass flow rates. For $\theta=27°$, $h=15$ mm ($q_*=61$, $u_l=0.66$ m/s), $\theta=33°h=14$ mm ($q_*=111$, $u_l=0.86$ m/s), for $\theta=37°h=8.1$ mm ($q_*=111$, $u_l=2.1$ m/s). Theoretical predictions are also reported: Savage's model [Eq. (1), with $e=0.63$, $\varphi=26.5°$, $u_l=3.5$ m/s], Mills *et al.*'s model [Eq. (3), with $\beta=0.0002$, $\varphi=26.5°$, $u_l=1.11$ m/s] are applied using $\theta=27°$ and $q_*=61$. Ancey and Evesque's model [Eq. (4), with $A=30$, $\varphi=26.5°$, $u_l=2.74$ m/s] is applied using $\theta=33°$ and $q_*=111$.

inclined channel was proposed by Savage [37]. He assumed that the bulk stress tensor can be divided into a frictional part and a collisional contribution. The former contribution is estimated using an empirical relationship derived from the Coulomb law used in soil mechanics. In a simple shear flow, this involves expressing the frictional shear stress as $\tau_f = p_o \sin\varphi$, where p_0 is called the mean quasistatic normal stress and will be computed from the motion equation. To estimate the collisional contribution, Savage used the kinetic theory developed by Jenkins and Savage [38], leading to an expression of the collisional shear stress in the form $\tau_c = 2\kappa(2+\lambda)\dot{\gamma}/5$, where $\dot{\gamma}$ denotes the shear rate, λ is a numerical coefficient reflecting the influence of anisotropy in the contact distribution ($\lambda \approx 1$), $\kappa = 2\phi^2(1+e)g_0\rho_p d\sqrt{T/\pi}$, with e the coefficient of restitution, $g_0(\phi)$ the radial distribution function, and T the granular temperature. From the equations of motion including a simplified set of boundary conditions (zero energy flux into the bed), Savage derived the velocity and density profiles as well as the discharge equations. He found that the velocity was a linear function of the flow depth:

$$u(y) = R\sqrt{3T_b}y/d, \tag{1}$$

where $R=\sqrt{10(1-e)/3}$ is a constant and T_b refers to the granular temperature at the channel bottom: $T_b = \phi g h \cos\theta/\{2(1+\varsigma)\phi_b^2(1+e)g_0(\phi_b)\}$, where ϕ_b denotes the density at the channel bottom and $\varsigma = [R\sqrt{27/(25\pi\tan^2\theta)} - 1](1-\sin\varphi/\tan\theta)^{-1}$. Thus the discharge equation is $q = R\sqrt{3T_b}h^2/(2d)$. We deduce that the discharge varies as $q \propto h^{5/2}$. The solid fraction satisfies the equation: $\phi^2 g_0(\phi) = (h-y)\phi_b^2 g_0(\phi_b)$. The inclination range for which a steady uniform flow takes place was found by Savage to be

$$\frac{\sin\phi}{2} + \frac{3}{10}\sqrt{\frac{10(1-e)}{\pi}} > \tan\theta > \sin\phi. \tag{2}$$

Further developments to Savage's theory were subsequently introduced by Johnson, Nott, and Jackson [11,40], Nott and Jackson [20], and Jackson [39]. They used a more sophisticated kinetic theory (Lun *et al.*'s model), more complete boundary conditions, and assumed that the normal force experienced by sustained contacts was a rational function of the solid fraction. In this way, the frictional contribution vanished as the solid fraction ϕ fell below a critical value and conversely as ϕ came closer to the maximum solid fraction, it had an increasing influence on bulk dynamics. Due to strong nonlinearities in boundary conditions and differential equations, the resulting equations of motion must be solved numerically [20]. Anderson and Jackson [41] have presented results in the case of a rough plane.

Mills, Loggia, and Tixier have modeled dry granular flows as motion of a network of transient solid chains through an assembly of particles behaving as a viscous or Bagnold (i.e., collisional regime) fluid [42,43]. In the latter case, they assumed that the collisional contribution can be written as $\tau_c = \beta\dot{\gamma}^2$, where β is a constant intrinsic to the material and the frictional contribution is given by the Coulomb law. Suggesting a further approximation of the interplay between the weak and strong populations, they arrived at the following velocity profile:

$$u(y) = \sqrt{\frac{\xi_x^3\rho g}{\beta}\cos\theta(\tan\theta - \tan\varphi)}\int_{(h-y)/\xi_x}^{h/\xi_x}\sqrt{1-e^{-z}}dz, \tag{3}$$

where ξ_x is the length correlation of the particle network (see Fig. 1), estimated at $\xi_x \approx \sqrt{hd}$. A velocity profile of this kind is almost linear except near the free surface. The density profile is assumed to be uniform across the entire flow depth. The discharge varies as $q \approx \sqrt{\rho g/(4\beta)}\sqrt{\cos\theta(\tan\theta-\tan\varphi)}(h^9 d)^{1/4} \propto h^{9/4}$. A steady uniform flow is then possible only if $\tan\theta \geqslant \tan\varphi$.

In the frictional-collisional model developed by Ancey and Evesque, the frictional and collisional contributions to bulk stress are tightly related and this interplay is governed by the Coulomb number [44]. Arguing that the strong population plays the key role in the stress generation mechanism (transmission of forces throughout the network of particles) while most of the shear work is dissipated within the weak population, the authors arrived at the conclusion that, for the frictional and collisional contribution to satisfy both the momentum and kinetic-energy balance equations, the energy dissipation rate must be constant on average. They also considered that a frictional-collisional regime—with the meaning $N_{Co}=O(1)$—cannot be achieved across the entire flow depth since a collisional boundary layer at the free surface and a frictional layer at the bottom should take place. In the region where the frictional-collisional regime is achieved, they found a logarithmic velocity profile

$$u(y)=-A\sqrt{dg\cos\theta(\tan\theta-k)}\,\ln(1-y/h), \qquad (4)$$

where $k=\tan\varphi$ in most cases [but $k=(1+2\tan^2\varphi)^{-1}$ is possible in some circumstances [2]], and A is a dimensionless parameter (intrinsic to the material). Close to the free surface, flow is collisional and the authors used a kinetic theory to compute the velocity profile:

$$u(y)=A\sqrt{dg\cos\theta(\tan\theta-k)}\,\ln\frac{h}{\delta}+\frac{14-6e}{\sqrt{\pi}}\frac{T_0^{3/2}}{gd\cos\theta}\times\left[1-\exp\left(-g\cos\theta\frac{y+d-h}{T_0}\right)\right], \qquad (5)$$

where $T_0=g\delta\cos\theta$ is the granular temperature at the collisional layer interface and δ is the thickness of the collisional layer, $\delta=d[A\bar{\phi}\tan\theta\sqrt{\tan\theta-k}/f_5(\bar{\phi})]^{2/3}$, where $f_5(\bar{\phi})=4(1-e^2)\bar{\phi}^2g_0(\bar{\phi})/\sqrt{\pi}$. The density profile is constant across the flow depth except in the collisional layer where it decreases exponentially towards zero. The total discharge is found to be

$$q=A\sqrt{dg\cos\theta(\tan\theta-k)}h\left(1+\frac{\delta}{h}\ln\frac{\delta}{h}-\frac{\delta}{h}\right). \qquad (6)$$

It is a linear increasing function of the flow depth for large flow depths while it decreases for flow depths of the order of the collisional layer thickness δ. A steady uniform flow occurs provided that the channel slope $\tan\theta$ lies in a limited range $[k,(k+A^{-2}C^{-1})]$, where C is a constant.

B. Comparison with experimental data

In our experiments, regime *A* was characterized by a discharge equation in the form $q\propto h^n$ with n in the range 2–3, a fairly linear velocity profile, and a slightly varying density profile. Qualitatively these points are well described by Savage's and Mills *et al.*'s models. However, for Anderson and Jackson's model, agreement with experimental data is partial. Indeed their numerical results (see Fig. 10 in Ref. [41]) show that for $h/d<10$, $n\approx2$, the velocity profiles were fairly linear (slight convexity), the solid fraction decreased slowly on moving up through the layer, and for $h/d>10$ the solid fraction decreased very quickly (mean solid concentration close to 0.3). The exponent n in the discharge equation given by Mills *et al.*'s model is 9/4, relatively close to the value $n=5/2$ found by Savage. As the experimental value of n varied in the range 2–3, it has not been possible to conclude which exponent gives better predictions. Savage's model has two input parameters. For the internal friction angle, we took the value found experimentally using a triaxial. We fitted the coefficient of restitution for the slope range of a steady flow [Eq. (2)] to match the experimental range. We found $e=0.63$. The lower the coefficient of restitution is, the wider the range of the steady flow is. Mills *et al.*'s model has a single input parameter β whose value was adjusted using a value of the mean velocity. We found: $\beta\approx2\times10^{-4}$ for 1-mm glass beads. For regime *A*, the density profile predicted by Savage's model was in good agreement with the experimental data except close to the free surface (see Fig. 17). The slight discrepancy at the free surface could be explained by the kinetic theory used in Savage's model, which neglects the kinetic contribution in the bulk stress tensor and thus should not be applied to dilute flows. In contrast, the assumption of uniform density made by Mills *et al.* was correct only at the channel bottom. As exemplified by Fig. 18, dimensionless velocity profiles provided by both models matched experimental data well. Comparison of the free-surface velocities shows that values u_{th} provided by the models are much larger than measured values $u_{expt.}$. For Mills *et al.*'s model, the ratio $u_{expt.}/u_{th.}$ was 0.55, in other words, very close to the reduction in velocity induced by sidewalls. However, for Savage's model, this ratio was 0.18; Savage's model overestimated the mean velocity by a factor of 3 for $\theta=27°$. We did not observe the change in the velocity profile curvature at the free surface predicted by Mills *et al.*'s model. However, the comparison could be biased because of wall effects and less accuracy in the measurements near the free surface. As the mean velocity depends on both the flow rate and the channel slope, it is not easy to infer the slope effect directly. In Fig. 19, we chose to plot the variation in the mean velocity for a given discharge (in regime *A*) as a function of the channel slope for different materials. Both experimental data and theoretical curves are reported; the input parameters were not altered. For 1-mm glass beads, velocities given by Mills *et al.*'s model are fairly close to experimental data over the range of slopes and discharges for which regime *A* took place. For 0.3-mm glass beads, velocities are slightly underestimated while for 2-mm glass beads, they are overestimated by a factor of 2. This may mean that the input parameter β depends on the bead size. In contrast, Savage's model fails to give the correct trend for the velocity variation with slope over the full range of slopes though it correctly predicts the order of magnitude of velocity for various discharges and materials without adjusting the coefficient of restitution.

Regime *B* was characterized by a discharge equation in the form $q\propto h^n$ (n in the range 0.94–1.14) and a convex linear velocity profile. The density profile in regime *B* is not very different from the one observed for regime *A*. Ancey

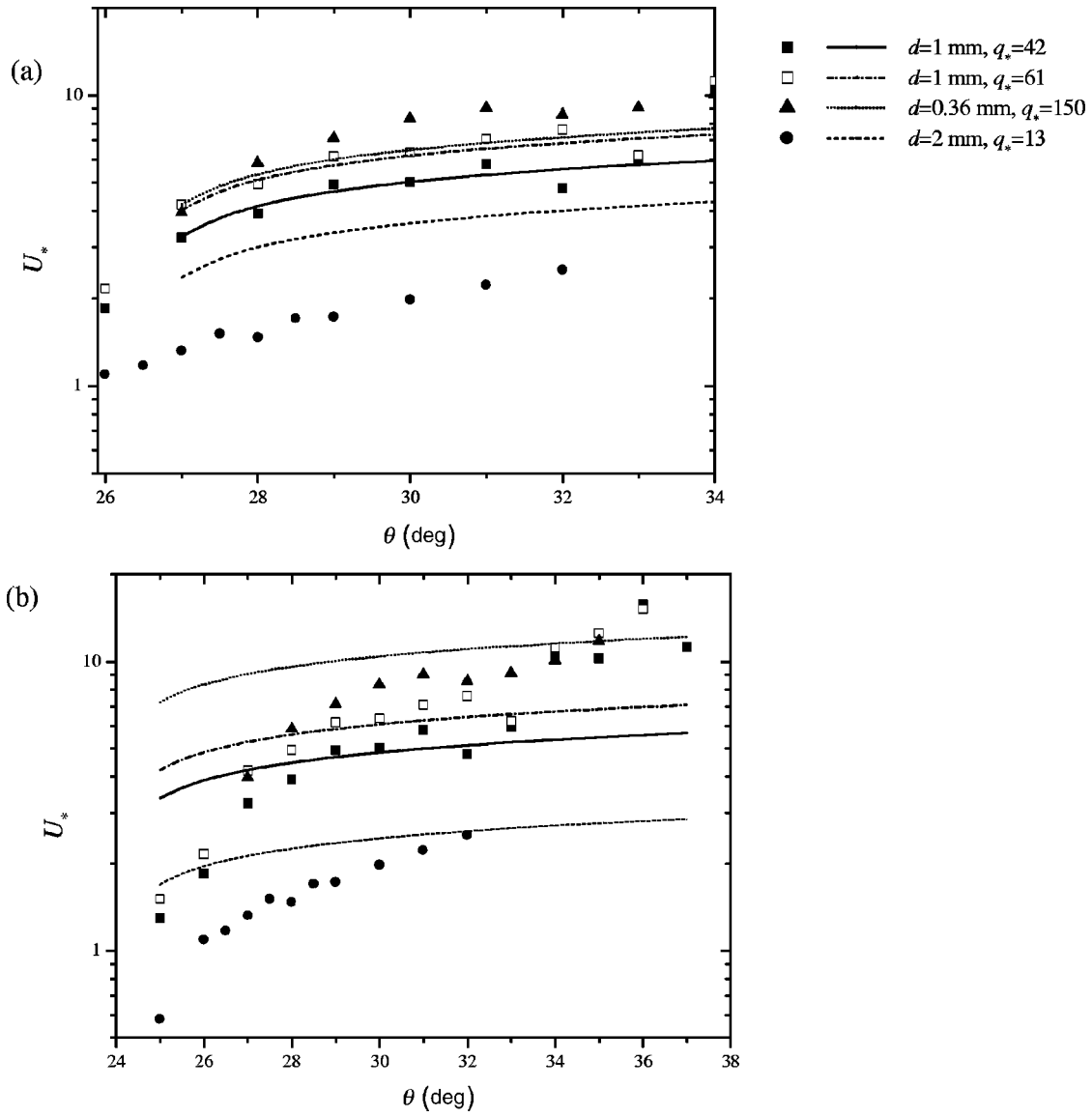

FIG. 19. Variation of the dimensionless velocity as a function of slope for a given flow rate and various materials. Experimental data are represented by squares, circles, and triangles. (a) Mills *et al.*'s model ($\beta=0.0002$, $\varphi=26.5°$). (b) Savage's model ($e=0.63$, $\varphi=26.5°$). The experimental data were taken from Figs. 9(a), 11(a), and 13(a).

and Evesque's model requires two input parameters: the internal friction angle, whose value was inferred from triaxial tests, and a dimensionless parameter A, whose value was estimated for each material by adjusting the mean theoretical velocity to the experimental data at a given slope $\theta=28°$. For large flow depths, the model provides a linear discharge equation or equivalently a constant mean velocity in agreement with the experimental data (see Figs. 8–13). The dependence of the mean velocity on the channel inclination is correctly predicted by this model for fine beads (0.36-mm and 1-mm glass beads), as shown in Fig. 15. For 0.36-mm glass beads in a narrow channel, the experimental curve varied almost linearly with the channel slope and thus the theoretical trend $U_* \propto \sqrt{\tan\theta - \tan\varphi}$ is not satisfied, as shown in Fig. 15. The model predicts that the velocity can be split into two parts: a lower part with a convex (logarithmic) velocity profile and an upper part, with a concave (exponential) velocity profile. It can be seen in Fig. 18 that the model slightly underestimates the reduced velocity $u(y)/u_l$ in the upper part of the velocity profile. Comparing the free-surface velocities shows that the theoretical value u_{th} was three times larger than the measured value $u_{expt.}$, while the expected ratio $u_{expt.}/u_{th.}$ (due to sidewall effects) was closer to 2. Moreover, in Fig. 18, the inflection point in the experimental velocity profile was approximately at $y/h \approx 0.8$ while the model located it at $y/h \approx 0.93$. This implies that the thickness of the collisional boundary layer at the free surface (δ) was also underestimated by the model. Furthermore, Fig. 17 shows that the density profile provided by this model was much more uniform than the one measured, which first decreased regularly for $0 \leqslant y/h \leqslant 0.8$, then decreased rapidly towards zero for $0.8 \leqslant y/h \leqslant 1$. This confirms that the collisional boundary layer was much thicker than predicted by the model.

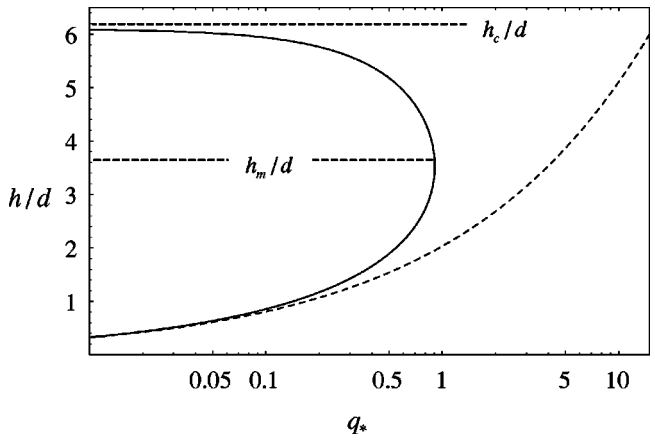

FIG. 20. Variation of the reduced flow depth as a function of the dimensionless flow rate. The continuous curve represents the full collisional model [Eq. (A9)] and the dashed curve Savage's frictional-collisional model. The following parameters have been used: $\theta=30°$, $e=0.63$, $e_w=0.99$, $\varphi=26.5°$, $\phi_b=0.66$. We found: $h_c=6.09$.

It is interesting to examine the reasons why a frictional-collisional regime should have two very different subregimes (A and B). A possible answer may be found by examining the role played by collisions. The appendix addresses the full collisional regime down an inclined channel. For comparison with Savage's frictional-collisional model, the same boundary conditions have been used. It is shown that for shallow flows, the flow rate q scales as $h^{5/2}$ but when the flow depth is raised to a critical value h_c (typically h_c has few diameters), the discharge curve is seen to rise to a maximum, then rapidly decrease to give zero flux at the value h_c. This means that the flow depth is a nonunique function of the flow rate (but the branch h_m-h_c in Fig. 20 is probably unstable). A typical example of variation is reported in Fig. 20. The same figure superimposes the predictions of Savage's frictional-collisional model. At low flow depths, the two curves coincide, but as the flow depth increases, the frictional-collisional model curve breaks away from that of the full collisional model and goes on rising monotonically. The same behavior was also obtained in the numerical simulations performed by Anderson and Jackson [41] using very different boundary conditions (smooth bottom) and a slightly different constitutive equation. As primarily pointed out by Anderson and Jackson [41], introducing a frictional term into the constitutive equation can eliminate apparent discrepancies appearing in a full collisional theory at high flow rates, even though bulk stress is mainly generated from collisions. It also has a physical significance since it is expected that in dense flows, the frictional contribution, whose magnitude is given by the flowing layer's own weight, has an increasing role in bulk dynamics as the flow depth increases. Finally, regime A can be considered as a frictional-collisional regime, in which collisions still play the key role in the bulk stress generation (whence the h^n scaling of the discharge curve, with n close to 5/2).

It has been experimentally observed that the transition to regime B is controlled by the Froude number. As is usual in instability of many free-surface gravity-driven flows, this could mean that the transition results from regime A's loss of stability. However, on the one hand, a linear stability analysis made using Mills *et al.*'s equation leads to a critical Froude number in the form: $\mathrm{Fr}_c=12\cos^{1/2}\theta/\sqrt{57}$, namely, a slightly decreasing function of the slope in contrast to experimental observations (see Fig. 16). On the other hand, the critical Froude number was not exceeded in our experiments while it should have if the transition results from a loss of linear stability. Ancey and Evesque have suggested that such a transition could be governed by the Coulomb number, but examination of their expression leads to a criterion in the form $N_{Co}\propto h/d<10$, in disagreement with the experimental data in Fig. 16. More probably the explanation lies in the existence of two different populations (strong and weak populations as depicted in Fig. 1) in regime B, leading to profound changes in the stress generation and distribution. Although no complete numerical simulations have so far been performed to elucidate this point, partial results have yielded valuable clues. Using a contact dynamics model, Prochnow and co-workers simulated a regime akin to regime A [8]. They found that the probability distribution of normal forces was a power function for weak forces and exponential for strong forces; moreover, the cutoff between these two populations was only slightly pronounced and the stress distribution was fairly uniform within the flowing layer. In contrast, using a similar numerical model to investigate a full frictional regime, Radjai *et al.* obtained a marked separation between weak and strong force distributions, leading to strong heterogeneity in stress distribution within the flowing layer [4]. Thus, in these simulations, the frictional contribution to bulk stress could be either diffuse throughout the layer or concentrated along force chains. It has been suggested that the transition from regime A to B results mainly from these changes in frictional stress generation.

Most theoretical models have found that the channel inclination must exceed the internal friction angle φ for steady uniform flows to occur. However, we observed steady uniform flows for channel slopes as low as 24° provided that the flow rate was not too high. At higher flow rates, the flow became unstable and a stationary wedge developed along the bed. No theoretical explanation has been provided to explain instability of this kind.

V. CONCLUDING REMARKS

In this paper, we have presented experimental investigations of dry granular flows down an inclined channel with a rough bottom. The observed flow pattern mainly depended on the channel inclination. Steady uniform flows, which were stable over a fairly wide range of flow rates, were observed for slopes exceeding the internal friction angle of the flowing material. Two regimes were identified. For shallow flows, the discharge equation was in the form $q\propto h^{5/2}$ and the velocity profile was approximately linear (regime A) in accordance with other experimental observations [27,29,33]. At high flow rates, the discharge was linear (regime B); the velocity profile was convex close to the channel bottom and concave near the free surface. Similar characteristics have also been observed by certain authors [22–25]. Other param-

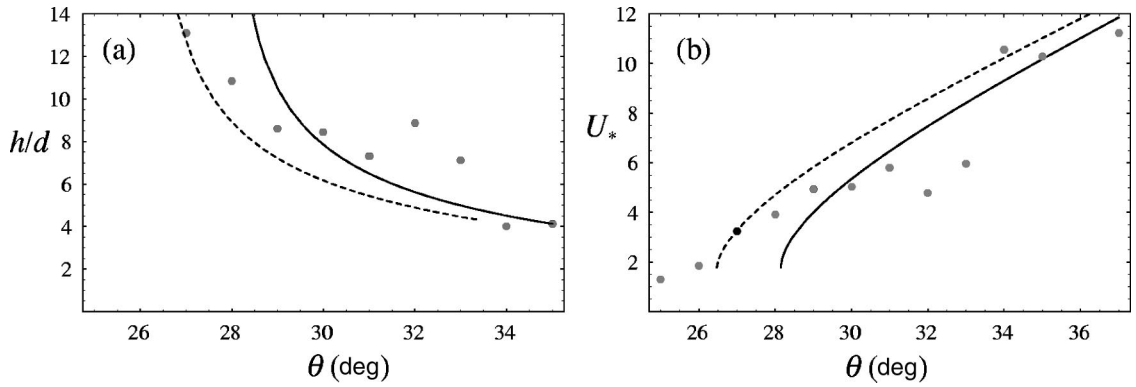

FIG. 21. Comparison of the full collisional model with experimental data. (a) Variation in the dimensionless velocity as a function of slope for a given flow rate $q_* = 42$, and 1-mm glass beads. Experimental data are represented by dots. (b) Variation in the dimensionless flow depth. The continuous curves correspond to $e = 0.85$ while the dashed curves were computed using $e = 0.87$. The experimental data were taken from Figs. 10(a) and 11(a).

eters such as the channel roughness or the particle diameter can affect the flow pattern to a varying extent. Different types of instability and transition were also observed. For channel inclinations lower than the internal friction angle, the flow became rapidly unstable and a stationary wedge developed along the bed. The transition from regime *A* to *B* could be either smooth or abrupt.

This paper has also presented a comparison between theoretical models and our experimental data. Savage's frictional-collisional model as well as Mills *et al.*'s empirical model provide results that capture the main flow features that we observed for regime *A*. This good agreement suggests that regime *A* is a frictional-collisional regime, where the collisional contribution imparts most of its features to bulk stress. For regime *B*, Ancey and Evesque's model yield satisfactory results. According to this model, regime *B* differs from regime *A* in that an increasing role is played by frictional contacts in bulk dynamics. Furthermore, comparison with recent numerical simulations (contact dynamics) suggests that the transition from regime *A* to *B* could reflect substantial changes in particle networks carrying frictional forces: in regime *A*, particle agitation limits the formation of chains with strong forces throughout the flowing layer. For regime *B*, the stress distribution within the bulk is controlled by the strong frictional force network while collisions are concentrated in clusters. Further numerical simulations should be performed to specify the way in which the transition from regime *A* to *B* occurs, and notably which criterion governs the transition.

ACKNOWLEDGMENTS

This study was supported by the Cemagref and funding was provided by the Institut National des Sciences de L'Univers of the CNRS (PNRN 99 29 CT). Additional support from the European program ''Debris Flow Risk'' (Grant No. ENV4-CT96-0253 DG12-D) is gratefully acknowledged. I am grateful to Pascal Moucheront, François Chevoir, Emmanuel Azanza, Jacques Terrières for their help in measuring the density profiles. I thank Philippe Coussot and Pierre Evesque for their valuable comments and encouragement. Michaël Prochnow provided Fig. 1. I also thank Stuart Savage, Hervé Capart, Luigi Fraccarolo, Michele Larcher, and Benoit Spierewine for valuable discussions that we had in the European Summer School held at Saint-Oyen.

APPENDIX

The appendix examines a purely collisional regime down an inclined channel in order to provide a fully analytical approximate solution; similar treatments can be found in the papers by Savage [37], Jenkins [45], and Anderson and Jackson [41]. Numerical simulations [46,47] have also been presented, but we do not refer to them here. We use the kinetic theory proposed by Jenkins and Savage [38], whose parameters have simple expressions, but as the treatment is rather general, alternative models may also be used. For kinetic theories, the constitutive equation has the following generic expression:

$$\Sigma_{col.}^{(p)} = -(p + \mu_v \boldsymbol{\nabla}\cdot\mathbf{u})\mathbf{1} + 2\mu\mathbf{D}, \tag{A1}$$

where p, μ_v, μ are respectively the pressure, bulk viscosity, and effective shear viscosity: $p = \rho_p f_1(\phi,e)T$, $\mu = \rho_p d f_2(\phi,e)\sqrt{T}$, $Q = -\rho_p d f_3(\phi,e) \times \sqrt{T}\boldsymbol{\nabla} T + \rho_p d f_4(\phi,e) T^{3/2}\boldsymbol{\nabla}\phi$, $\dot{\varepsilon} = \rho_p / d f_5(\phi,e) T^{3/2}$, where Q denotes the pseudothermal energy flux and $\dot{\varepsilon}$ the energy sink. As usual, we assume that $f_4 = 0$. In addition to the momentum equation, the energy balance equation is needed:

$$\frac{3}{2}\rho\frac{dT}{dt} = \mathrm{tr}(\Sigma_{col.}^{(p)}\mathbf{D}) - \boldsymbol{\nabla}\cdot\mathbf{Q} - \dot{\varepsilon}. \tag{A2}$$

We assume that the flow is sufficiently dense for the local concentration to be close to its mean value $\overline{\phi}$. In a simple shear velocity, the velocity u is in the form $(0,u(y),0)$. Thus the continuity equation is systematically satisfied. A complete and clearly validated formulation of boundary conditions (at a solid wall) is still lacking: complicated and coupled phenomena (such as torque transmission, depletion, propagation of elastic waves through the bumpy bottom sur-

face [48]) certainly affect the energy balance, but the question of how they interact is quite confused. In most available theoretical treatments, the energy balance is deduced from heuristic considerations and thus involves a series of empirical (indeterminate) parameters. Here we simply assume that the energy balance given by Eq. (A2) still holds true, but, in accordance with studies on the motion of a single particle down a bumpy line [49], it is thought that inelastic dissipation acts as the main sink for granular temperature. Therefore, as a first approximation, we neglect the influence of the thermal energy flux (Q) in the energy balance equation. Finally, we obtain: $\tau_0 \dot{\gamma}_0 = \dot{\varepsilon}_{y=0}$, where the subscript 0 refers to the wall position ($y=0$). The coefficient of restitution (at the wall) e_w is normally different from the one used in equations of motion. In addition, we have to specify the slip velocity at the bottom surface. Generally, this velocity can be inferred from the momentum balance equation (in the vicinity of the wall). As a first approximation, since these momentum considerations generally lead to a slip velocity expression in the form $u_0 \propto R\dot{\gamma}_0 \propto \sqrt{T_0}$, we can neglect it in comparison with the mean flow velocity: $u_0 \approx 0$. Concerning the boundary conditions at the free surface, it is admitted that the stress and gradient of thermal energy flux vanish. In the Jenkins-Savage model, the functions f_i are written as $f_i(\phi,e) = \alpha_i f(\phi,e)$, with $\alpha_1 = 1$, $\alpha_2 = 2(2+\alpha_0)/(5\sqrt{\pi})$, $\alpha_3 = 1/\sqrt{\pi}$, $\alpha_4 = 0$, and $\alpha_5 = 6(1-e)/\sqrt{\pi}$, where α_0 denotes a parameter accounting for anisotropy in the collisional contact distribution ($\alpha_0 = 1/\sqrt{\pi}$ here). We have also introduced $f(\phi,e) = 2(1+e)\phi^2 g_0(\phi)$ and Carnahan and Starling's expression for the radial distribution function $g_0(\phi) = (1 - \phi/2)/(1-\phi)^3$.

We are looking for a solution to equations of motion in the case of a steady uniform flow down a rough plane. As the normal and shear stresses are given by: $\tau = \overline{\rho} g(h-y)\sin\theta$ and $\sigma = -\overline{\rho} g(h-y)\cos\theta$, we directly deduce the shear rate,

$$\dot{\gamma} = \frac{f_1}{f_2}\frac{\tan\theta}{d}\sqrt{T}. \tag{A3}$$

With our assumption of large flow density, it is possible to express the granular temperature as $fT = \overline{\rho} g(h-y)\cos\theta/\rho_p$. Using this relationship and the proportionality between the normal and shear stresses ($\tau = -\sigma\tan\theta$), we deduce from the energy balance equation (A2) that

$$0 = \phi\rho_p g(h-y)\sin\theta\frac{f_1}{f_2}\frac{\tan\theta}{d}\sqrt{T} + 2\frac{d}{dy}\rho_p d\alpha_3 fT\frac{d}{dy}\sqrt{T} - \frac{\rho_p}{d}\alpha_5 fT^{3/2}. \tag{A4}$$

Introducing the thermal velocity $w = \sqrt{T}$ and substituting fT by $\overline{\rho} g(h-y)\cos\theta/\rho_p$, we obtain

$$w'' - \frac{w'}{h-y} + Fd^{-2}w = 0 \tag{A5}$$

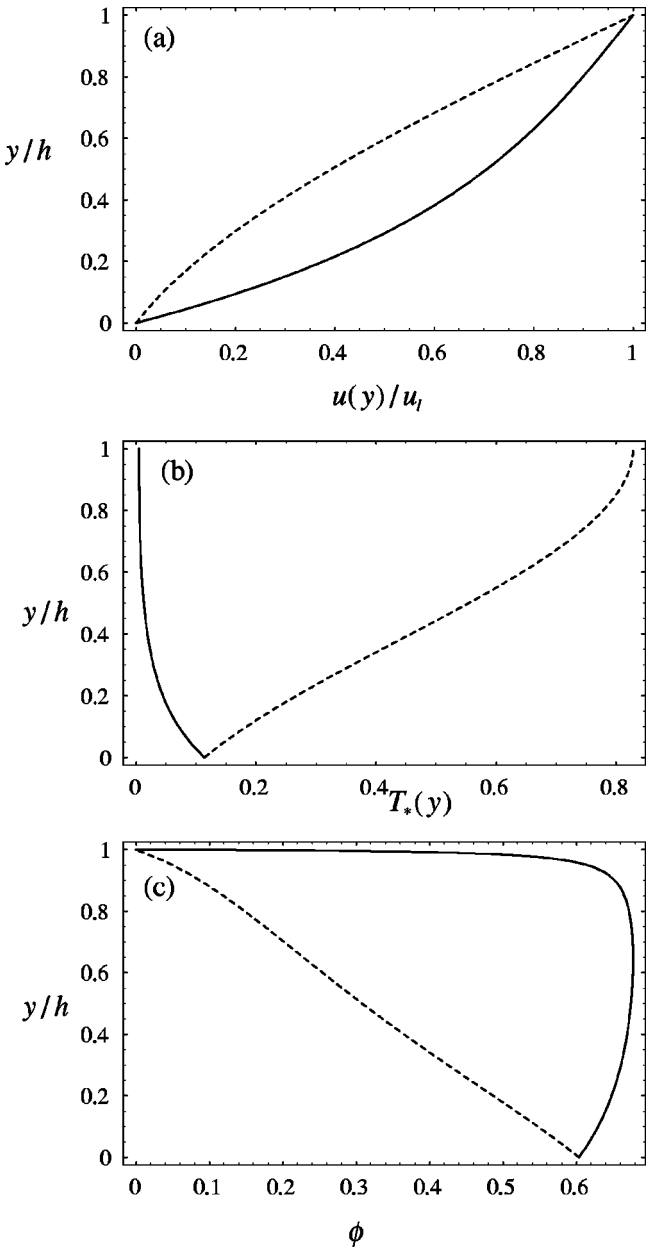

FIG. 22. Predictions of the full collisional model down an inclined rough plane. (a) Profile of the dimensionless velocity. (b) Profile of the dimensionless temperature. (c) Profile of the solid fraction. Calculations made for $\theta = 30°$ and $h = 10d$. The continuous curves correspond to $e = 0.8$ ($F<0$) while the dashed curves were computed for $e = 0.84$ ($F>0$).

with $F = (\alpha_1\tan^2\theta/\alpha_2 - \alpha_5)/(2\alpha_3)$. The solution depends on the sign of F. For plane inclinations in excess of a critical value, $\theta > \theta_c = \arctan\sqrt{\alpha_1^{-1}\alpha_5\alpha_2}$, F is positive. We find $\theta_c = \arctan\sqrt{12(2+\alpha_0)(1-e)/(5\pi)}$ in the Jenkins-Savage theory. In this case, we can express the thermal velocity in terms of the Bessel function of the first kind of order 0 (J_0),

$$w(y) = w_0\frac{J_0(\sqrt{F}(h-y)/d)}{J_0(\sqrt{F}h/d)}. \tag{A6}$$

Due to the oscillatory nature of J_0 (J_0 can be negative), Eq. (A6) is meaningful provided that $\sqrt{F}h<\xi_0 d$, where ξ_0 is the first root of J_0 ($\xi_0\approx 2.40$). For $F<0$ the solution can be written as

$$w(y)=w_0\frac{I_0(\sqrt{|F|}(h-y)/d)}{I_0(\sqrt{|F|}h/d)}, \tag{A7}$$

where I_0 is the modified Bessel function of the first kind of order 0. The thermal velocity at the wall is determined by the boundary equation ($\tau_0\dot{\gamma}_0=\dot{\varepsilon}_{y=0}$): $w_0=\sqrt{\bar{\phi}}gh\sin^2\theta\cos^{-1}\theta f_1(\phi_0)f_5^{-1}(\phi_0)f_2^{-1}(\phi_0)$. The boundary conditions at the free surface are systematically satisfied for both solutions. From Eq. (A7), we directly deduce the velocity after integration:

$$u=\frac{w_0\tan\theta}{\vartheta}\frac{f_1}{f_2}\frac{h}{d}\left[H\left(\frac{1}{2};1,\frac{3}{2};-\frac{h^2}{d^2}\frac{F}{4}\right)-\frac{h-y}{h}H\left(\frac{1}{2};1,\frac{3}{2};-\frac{(h-y)^2}{d^2}\frac{F}{4}\right)\right], \tag{A8}$$

where H is the hypergeometric differential function, $\vartheta=I_0(\sqrt{|F|}h/d)$ for $F<0$ and $\vartheta=J_0(\sqrt{F}h/d)$ for $F>0$. An expansion into a second order series leads to $u(y)\propto y+o(y^3)$, which indicates that the velocity profile is almost linear for shallow flows. For thick flows, the velocity profile $u(y)$ is convex for $F>0$ and concave for $F<0$ (it is linear for $F=0$). For very large negative values of F, the velocity profile exhibits a plug flow: only layers near the bed are sheared while the upper part of the flow moves as a rigid block. For h/d in excess of about 10, the velocity profile is no longer linear and a nonsheared zone takes place at the free surface. A new integration leads to the discharge equation

$$q=\frac{w_0\tan\theta}{2\vartheta}\frac{f_1}{f_2}\frac{h^2}{d}\left[2H\left(\frac{1}{2};\frac{3}{2},2;-\frac{F}{4}\frac{h^2}{d^2}\right)-H\left(\frac{1}{2};1,\frac{3}{2};-\frac{F}{4}\frac{h^2}{d^2}\right)\right]. \tag{A9}$$

For the flow rate to be positive in the case $F<0$, the flow depth must satisfy the condition $\sqrt{F}h<2\xi_1 d$, where ξ_1 is the first root of H ($\xi_1\approx 5.57$). A series expansion to chief order leads to the simplified expression of the mass flow rate versus inclination and flow depth: $q\approx\tan\theta\sqrt{\cos\theta}M\sqrt{g}h^{5/2}/d$, where M is a dimensionless parameter, $M=\sqrt{\bar{\phi}f(\bar{\phi})}/(4\alpha_5\alpha_2^3)$. When compared to our experimental data, the full collisional model provides satisfactory trends and order of magnitude, as exemplified in Fig. 21. One of the major issues in this model is the great sensitivity of results with respect to initial parameters and boundary conditions. In Fig. 22, we have reported examples of velocity profiles, granular temperature distributions, and solid concentration profiles for two values of the coefficient of restitution ($e=0.8$ and $e=0.84$). It clearly appears that significant differences are caused by minute changes (5%) in the coefficient of restitution. For $e=0.84$, the solid concentration profile decreases strongly towards zero on moving up through the layer, which is inconsistent with the dense flow assumption. As most flow conditions satisfying $F>0$ lead to such profiles, the physical meaning of this solution may be questioned. Moreover, the solution associated with $F>0$ implies that the flow depth does not exceed a critical value $h<h_c=F^{-1/2}\xi_0 d$. The results are very sensitive to the type of boundary conditions, especially for shallow flows. This is normal since the boundary conditions specify the manner in which energy is put into the flow through the bed. Here, like Savage [37], we addressed the case of zero energy flux into the bed and that is why we obtained analogous results. Using a diffusive process as boundary conditions, Anderson and Jackson [41] and Jenkins [45] found that the flow depth was independent of the discharge and equal to h_c.

[1] S. B. Savage, Adv. Appl. Mech. **24**, 289 (1984).
[2] C. Ancey, P. Coussot, and P. Evesque, J. Rheol. **43**, 1673 (1999).
[3] M. A. Schofield and C. P. Wroth, *Critical State of Soil Mechanics* (McGraw-Hill, London, 1968).
[4] F. Radjai, D. E. Wolf, M. Jean, and J. J. Moreau, Phys. Rev. Lett. **80**, 61 (1998).
[5] F. Radjai and D. Wolf, Granular Matter **1**, 3 (1998).
[6] R. A. Bagnold, Proc. R. Soc. London, Ser. A **225**, 49 (1954).
[7] C. S. Campbell, Annu. Rev. Fluid Mech. **22**, 57 (1990).
[8] M. Prochnow, F. Chevoir, P. Mills, and J. T. Jenkins, in *Physique et Mécanique des Matériaux Granulaires, Champ-sur-Marne, 2000* (Presses du LCPC, Paris, 2000), p. 425.
[9] H. Capart, L. Fraccarolo, L. Guarino, A. Armanini, and Y. Zech, in *Debris Flow Conference, Taipei (Taiwan), 2000*, edited by G. F. Wieczorek and N. D. Naesser (Balkema, Rotterdam, 2000), p. 361.
[10] E. Aharonov and D. Sparks, Phys. Rev. E **60**, 6890 (1999).
[11] P. C. Johnson, P. Nott, and R. Jackson, J. Fluid Mech. **210**, 501 (1990).
[12] K. Ridgway and R. Rupp, Chem. Process Eng. (London) **51**, 82 (1970).
[13] H. Ahn, C. E. Brennen, and R. H. Sabersky, J. Appl. Mech. **58**, 792 (1991).
[14] K. Takahasi, Geophys. Mag. **11**, 165 (1937).
[15] D. A. Augenstein and R. Hogg, Powder Technol. **10**, 43 (1974).
[16] C. S. Campbell, C. E. Brennen, and R. H. Sabersky, Powder Technol. **41**, 77 (1985).
[17] C. E. Brennen, K. Sieck, and J. Palaski, Powder Technol. **35**, 31 (1983).
[18] J. S. Patton, C. E. Brennen, and R. H. Sabersky, J. Appl. Mech. **54**, 801 (1987).
[19] O. Hungr and R. R. Morgenstern, Geotechnique **34**, 405 (1984).
[20] P. Nott and R. Jackson, J. Fluid Mech. **241**, 125 (1992).

[21] S. N. Prasad, D. Pal, and J. M. Römkens, J. Fluid Mech. **413**, 89 (2000).
[22] A. Suzuki and T. Tanaka, Ind. Eng. Chem. Fundam. **10**, 84 (1971).
[23] S. B. Savage, J. Fluid Mech. **92**, 53 (1979).
[24] M. Ishida, H. Hatano, and T. Shirai, Powder Technol. **27**, 7 (1980).
[25] M. Ishida and H. Hatano, in *Advances in the Mechanics and the Flow of Granular Materials*, edited by M. Shahinpoor (Trans Tech Publications, Clausthal-Zellerfeld, 1983), p. 565.
[26] M. Ishida, H. Hatano, and T. Shirai, Powder Technol. **27**, 1 (1980).
[27] J. W. Vallance, Ph.D. thesis, Michigan Technology University, 1994.
[28] C. Ancey, P. Coussot, and P. Evesque, Mech. Cohesive-Frict. Mater. **1**, 385 (1996).
[29] O. Pouliquen, Phys. Fluids **11**, 542 (1999).
[30] D. M. Hanes and O. R. Walton, Powder Technol. **109**, 133 (2000).
[31] T. G. Drake, J. Fluid Mech. **225**, 121 (1991).
[32] T. G. Drake, J. Geophys. Res. [Solid Earth Planets] **95**, 8691 (1990).
[33] E. Azanza, F. Chevoir, and P. Moucheront, J. Fluid Mech. **400**, 199 (1999).
[34] R. M. Nedderman, U. Tüzün, S. B. Savage, and G. T. Houlsby, Chem. Eng. Sci. **37**, 1597 (1982).
[35] V. T. Chow, *Open-Channel Hydraulics* (McGraw-Hill, Singapore, 1959).
[36] S. A. Tan and T. F. Fwa, Geotech. Test **14**, 257 (1991).
[37] S. B. Savage, in *U.S./ Japan Seminar on New Models and Constitutive Relations in the Mechanics of Granular Materials, Ithaca, 1982*, edited by J. T. Jenkins and M. Satake (Elsevier Science Publishers, Amsterdam, 1982), p. 261.
[38] J. T. Jenkins and S. B. Savage, J. Fluid Mech. **130**, 187 (1983).
[39] R. Jackson, J. Rheol. **30**, 907 (1986).
[40] P. C. Johnson and R. Jackson, J. Fluid Mech. **176**, 67 (1987).
[41] K. G. Anderson and R. Jackson, J. Fluid Mech. **241**, 145 (1992).
[42] P. Mills, D. Loggia, and M. Tixier, Europhys. Lett. **45**, 733 (1999).
[43] P. Mills, D. Loggia, and M. Tixier, J. Phys. E **1**, 5 (2000).
[44] C. Ancey and P. Evesque, Phys. Rev. E **62**, 8349 (2000).
[45] J. T. Jenkins, Appl. Mech. Rev. **47**, 240 (1994).
[46] S. Abu-Zaid and G. Ahmadi, Powder Technol. **77**, 7 (1993).
[47] T. Scheiwiller and K. Hutter, in *Advances in the Mechanics and the Flow of Granular Materials* (Ref. [25]), p. 613.
[48] C. S. Campbell, J. Fluid Mech. **247**, 137 (1993).
[49] C. Ancey, P. Evesque, and P. Coussot, J. Phys. I **6**, 725 (1996).